

High-scale validity of a model with Three-Higgs-doublets

Nabarun Chakrabarty^{†1}

[†]*Regional Centre for Accelerator-based Particle Physics*

Harish-Chandra Research Institute

Chhatnag Road, Jhansi, Allahabad - 211 019, India

Abstract

We consider a three-Higgs doublet scenario in this paper, invariant under the discrete group S_3 , and probe its high-scale validity by allowing the model parameters to evolve under renormalisation group. We choose two particular alignments of vacuum expectation values (vev) for our study, out of a set of several such possible ones. All three doublets receive non-zero vacuum expectation values in the first case, and in the second case, two of the doublets remain without vev. The constraints on the parameter space at low energy, including the measured value of the Higgs mass and the signal strengths, oblique corrections and also measurements of relic density and direct detection rates are juxtaposed with the conditions of vacuum stability, perturbativity and unitarity at various scales. We find that the scenario with three non-zero vevs is not valid beyond 10^7 GeV, assuming no additional physics participates at the intermediate scales. On the contrary, the scenario with only one non-zero vev turns out to be a successful model for cold dark matter phenomenology, which also turns out to be valid up to the Planck scale at the same time. Stringent restrictions are obtained on the model parameter space in each case. Thus, the S_3 symmetric scalar sector emerges as an ultraviolet (UV) complete theory.

¹nabarunc@hri.res.in

1 Introduction

The discovery of a scalar boson around 125 GeV [1, 2] has been the most important finding at the LHC so far. It has gradually unfurled that the newly discovered boson has properties largely consistent with the Standard Model (SM) Higgs [3–5]. There is however one pressing issue that a SM Higgs around 125 GeV leads to an instability in the electroweak vacuum around 10^{8-9} GeV if the top quark mass (M_t) and the strong coupling constant (α_s) are on the upper edges of their respective uncertainty bands. A recent next-to-next-to-leading order (NNLO) study [6, 7] reports that absolute stability up to the Planck scale requires

$$M_h[\text{GeV}] > 129.4 + 1.4\left(\frac{M_t[\text{GeV}] - 173.1}{0.7}\right) - 0.5\left(\frac{\alpha_s(M_Z) - 0.1184}{0.0007}\right) \pm 1.0_{\text{th}} \quad (1.1)$$

As a possible remedy to alleviate the vacuum stability problem, the SM Higgs can be made to couple to additional bosonic degrees of freedom. In such a case, the extra scalar loops contributing to the running of the Higgs coupling can generate the required positive contribution to prevent the Higgs self coupling from turning negative. Thus ensuring a stable Electroweak vacuum (EW) up to the GUT and Planck scales, forms our main motivation to add new scalars to the theory. Apart from this, various cosmological and astrophysical evidences of Dark Matter (DM) also necessitate physics beyond the SM. Attempts have been made to explore the yet unknown particle nature of DM and the most successful proposal is that DM is constituted of Weakly Interacting Massive Particles (WIMPs) [8].

It is however not possible to predict the actual number of scalar doublets present in nature from fundamental principles. The discovered scalar resonance around 125 GeV could very well arise from a multiple scalar doublet scenario with the additional parameters arranged suitably to give to it, SM-like couplings to fermions and gauge bosons. Of course, detection of the extra scalars at the colliders is the only direct way to pin down on the exact scalar structure present. Nonetheless these extra scalars could be fingerprinted through their role in stabilizing and unitarizing of the scalar potential. Moreover, the scalars originating from the extra doublets could possibly be successful candidates for DM. While studies combining together vacuum stability and DM phenomenology have been done in the past in context of two-Higgs doublet models (2HDM) [9], these could be generalized to a higher number of doublets as well. There has been a rising interest in three-Higgs doublet models (3HDM) in the recent past [10–20]. The chief phenomenological motivation of which is that the existence of three scalar doublets, replicating the three fermion families, sheds light on the flavor problem. 3HDMs have rather wide scalar spectrum. In fact, invariance under $SU(2) \times U(1)$ tells us that there are four neutral scalars, and a pair of charged scalars obtainable from a generic 3HDM. It is reminded that 3HDMs come in various types, depending upon the global symmetry present. One of them is the 3HDM endowed with a global S_3 symmetry [21–26]. This S_3 symmetry is already important from the perspective of flavor, it reproduces the lepton masses and mixings accurately [27–32]. The scalar sector is also interesting since there is an economy of parameters compared to a more generic 3HDM. In fact the eight dimensionless parameters can be fully traded off in favour of the seven masses and one mixing angle. The S_3 -symmetric scalar sector has spurred some investigation in the past, and some standalone studies related to DM phenomenology have also occurred [33]. However, the present study is mainly directed towards analysing the Higgs sector, and, it includes the following features which have not been highlighted before.

- We derive the renormalisation group equations at one-loop for the dimensionless parameters in an S_3 symmetric Higgs potential. Using these, we probe high-scale behaviour of the scalar potential. That

is, we evolve the scalar quartic couplings and require that the model remains perturbative and keeps vacuum stability intact at each intermediate energy scale. Through this exercise, we try to identify the parameter space at the input scale that keeps the model *valid* till very high scales.

- Electroweak Symmetry Breaking (EWSB) is triggered when one or more doublet receives a vacuum expectation value (vev). While several such configurations of the vevs can be there in principle, we consider two such cases which not only are more relevant from the phenomenological point of view, but also demonstrative of the high-scale validity of the S_3 potential. For instance, we analyse a 'two inert doublet' scenario where only one doublet gets a vev, and predicts existence of stable scalars through some remnant symmetry. This scenario thus stands as a potential candidate for describing DM.
- The parameter space allowing for high-scale validity is also subject to various *low energy* constraints, i.e., the ones originating from the oblique S, T and U parameters, signal strength measurements for the 125 GeV Higgs, and also DM searches.

This paper is organized as follows. In Section 2, we briefly discuss the salient features of the model, particularly the scalar and Yukawa sectors. The various constraints taken are listed in Section 3. The numerical results so obtained are detailed in Section 4, and finally, we summarize in Section 5. Relevant expressions and equations can be found in the Appendix 6.

2 The S_3 symmetric three-Higgs-doublet model (S_3 HDM) in brief.

2.1 Scalar sector.

The scalar sector consists of three scalar doublets ϕ_1 , ϕ_2 and ϕ_3 . The most general renormalizable scalar potential consistent with the gauge and S_3 symmetries can be cast as [34],

$$\begin{aligned}
V(\phi) = & \mu_{11}^2(\phi_1^\dagger\phi_1 + \phi_2^\dagger\phi_2) + \mu_{33}^2\phi_3^\dagger\phi_3 \\
& + \lambda_1(\phi_1^\dagger\phi_1 + \phi_2^\dagger\phi_2)^2 + \lambda_2(\phi_1^\dagger\phi_2 - \phi_2^\dagger\phi_1)^2 + \lambda_3 \left\{ (\phi_1^\dagger\phi_2 + \phi_2^\dagger\phi_1)^2 + (\phi_1^\dagger\phi_1 - \phi_2^\dagger\phi_2)^2 \right\} \\
& + \lambda_4 \left\{ (\phi_3^\dagger\phi_1)(\phi_1^\dagger\phi_2 + \phi_2^\dagger\phi_1) + (\phi_3^\dagger\phi_2)(\phi_1^\dagger\phi_1 - \phi_2^\dagger\phi_2) + \text{h.c.} \right\} \\
& + \lambda_5(\phi_3^\dagger\phi_3)(\phi_1^\dagger\phi_1 + \phi_2^\dagger\phi_2) + \lambda_6 \left\{ (\phi_3^\dagger\phi_1)(\phi_1^\dagger\phi_3) + (\phi_3^\dagger\phi_2)(\phi_2^\dagger\phi_3) \right\} \\
& + \lambda_7 \left\{ (\phi_3^\dagger\phi_1)(\phi_3^\dagger\phi_1) + (\phi_3^\dagger\phi_2)(\phi_3^\dagger\phi_2) + \text{h.c.} \right\} + \lambda_8(\phi_3^\dagger\phi_3)^2.
\end{aligned} \tag{2.1a}$$

A 3HDM is usually known to have CP violating phases [35] in the scalar sector. For example a complex λ_4 and λ_7 in this case leads to CP non-conservation, although the phases are severely constrained by measurements of Electric Dipole Moment of the Neutron (EDMN) [36]. The high-scale stability of a 2HDM is found intact regardless of the CP phase [37]. Thus, the overall conclusions regarding validity of the S_3 HDM at high scales is expected to remain unaffected by the introduction of CP phases. So we choose λ_4 and λ_7 to be real henceforth.

Electro-Weak Symmetry Breaking (EWSB) assigns vacuum expectation values (vevs) v_1 , v_2 and v_3 to the doublets ϕ_1 , ϕ_2 and ϕ_3 respectively. However, they all are not independent as the S_3 invariance forces

relationships among them through the minimization conditions below,

$$2\mu_{11}^2 = -2\lambda_1(v_1^2 + v_2^2) - 2\lambda_3(v_1^2 + v_2^2) - v_3\{6\lambda_4 v_2 + (\lambda_5 + \lambda_6 + 2\lambda_7)v_3\}, \quad (2.2a)$$

$$2\mu_{11}^2 = -2\lambda_1(v_1^2 + v_2^2) - 2\lambda_3(v_1^2 + v_2^2) - \frac{3v_3}{v_2}\lambda_4(v_1^2 - v_2^2) - (\lambda_5 + \lambda_6 + 2\lambda_7)v_3^2, \quad (2.2b)$$

$$2\mu_{33}^2 = \lambda_4 \frac{v_2}{v_3}(v_2^2 - v_1^2) - (\lambda_5 + \lambda_6 + 2\lambda_7)(v_1^2 + v_2^2) - 2\lambda_8 v_3^2. \quad (2.2c)$$

The self-consistency of Eqs. (2.2a) and (2.2b) gives rise to the following possibilities,

$$\lambda_4 = 0, \quad (2.3a)$$

$$\text{or, } v_1 = \sqrt{3}v_2, \quad (2.3b)$$

$$\text{or, } v_1 = v_2 = 0, \ v_3 = 246 \text{ GeV}. \quad (2.3c)$$

The first case causes a physical scalar to turn massless as reported in [38]. This directs us towards the other two cases that we outline below.

The doublets are parameterized in the following fashion,

$$\phi_i = \frac{1}{\sqrt{2}} \begin{pmatrix} \sqrt{2}w_i^+ \\ v_i + h_i + iz_i \end{pmatrix} \text{ for } i = 1, 2, 3. \quad (2.4)$$

The physical scalar spectrum of a generic CP-conserving 3HDM consists of three CP even neutral scalars, H_1 , H_2 and h ; two CP-odd neutral scalars A_1 and A_2 ; and two charged scalars H_1^+ and H_2^+ . We define $\tan\beta = \frac{2v_2}{v_1}$ for Scenario A (Eqn.2.3b). For this vev-alignment, only two mixing angles α and β are sufficient to parameterize the transformation matrices connecting the SU(2) eigenbasis to the physical basis, somewhat resembling a 2HDM.¹ The model is more conveniently described in terms of physical quantities like masses and mixing angles. The eight λ_i can be traded for the seven masses and the mixing angle α (See [39] for definition.) using the following equations,

$$\lambda_1 = \frac{1}{2v^2 \sin^2 \beta} \left\{ (m_h^2 \cos^2 \alpha + m_{H_1}^2 \sin^2 \alpha) + \left(m_{H_1^+}^2 - m_{H_2^+}^2 \cos^2 \beta - \frac{1}{9} m_{H_2}^2 \right) \right\}, \quad (2.5a)$$

$$\lambda_2 = \frac{1}{2v^2 \sin^2 \beta} \left\{ (m_{H_1^+}^2 - m_{A_1}^2) - (m_{H_2^+}^2 - m_{A_2}^2) \cos^2 \beta \right\}, \quad (2.5b)$$

$$\lambda_3 = \frac{1}{2v^2 \sin^2 \beta} \left(\frac{4}{9} m_{H_2}^2 + m_{H_2^+}^2 \cos^2 \beta - m_{H_1^+}^2 \right), \quad (2.5c)$$

$$\lambda_4 = -\frac{2}{9} \frac{m_{H_2}^2}{v^2} \frac{1}{\sin \beta \cos \beta}, \quad (2.5d)$$

$$\lambda_5 = \frac{1}{v^2} \left\{ \frac{\sin \alpha \cos \alpha}{\sin \beta \cos \beta} (m_{H_1}^2 - m_h^2) + 2m_{H_2^+}^2 + \frac{1}{9} \frac{m_{H_2}^2}{\cos^2 \beta} \right\}, \quad (2.5e)$$

$$\lambda_6 = \frac{1}{v^2} \left(\frac{1}{9} \frac{m_{H_2}^2}{\cos^2 \beta} + m_{A_2}^2 - 2m_{H_2^+}^2 \right), \quad (2.5f)$$

$$\lambda_7 = \frac{1}{2v^2} \left(\frac{1}{9} \frac{m_{H_2}^2}{\cos^2 \beta} - m_{A_2}^2 \right), \quad (2.5g)$$

$$\lambda_8 = \frac{1}{2v^2 \cos^2 \beta} \left\{ (m_h^2 \sin^2 \alpha + m_{H_1}^2 \cos^2 \alpha) - \frac{1}{9} m_{H_2}^2 \tan^2 \beta \right\}. \quad (2.5h)$$

¹A more detailed discussion regarding the transformation matrices can be found in [39].

We also put forth the Scenario B (Eqn.2.3c) as an alternate symmetry breaking pattern. In this case, ϕ_3 is the only active doublet, which is in fact a singlet under S_3 . Consequently, all the fermions couple to ϕ_3 alone and thus they too are S_3 -singlets. The remaining doublets ϕ_1 and ϕ_2 remain *inert*. A Z_2 symmetry is found unbroken for $\lambda_4 = 0$, and it forbids mixing among scalars coming from different doublets thus enabling one to express the doublets directly in terms of the physical fields as,

$$\phi_3 = \frac{1}{\sqrt{2}} \begin{pmatrix} \sqrt{2}w^+ \\ v + h + iz \end{pmatrix} \quad (2.6)$$

$$\phi_i = \frac{1}{\sqrt{2}} \begin{pmatrix} \sqrt{2}H_i^+ \\ H_i + iA_i \end{pmatrix} \text{ for } i = 1, 2. \quad (2.7)$$

With $m_h^2 = 2\lambda_8 v^2$ now, the S_3 symmetry leads to a mass degeneracy in the inert sector,

$$m_{H_1}^2 = m_{H_2}^2 = \mu_{11}^2 + \frac{1}{2}\lambda_L v^2 \quad (2.8)$$

$$m_{A_1}^2 = m_{A_2}^2 = \mu_{11}^2 + \frac{1}{2}\lambda_A v^2 \quad (2.9)$$

$$m_{H_1^+}^2 = m_{H_2^+}^2 = \mu_{11}^2 + \frac{1}{2}\lambda_5 v^2 \quad (2.10)$$

Here $-\lambda_L v$ and $-\lambda_A v$ denote the H_1 - H_1 - h and A_1 - A_1 - h couplings respectively. This mass degeneracy can be lifted in this case, for example, by introducing an S_3 breaking quadratic term of the form $-\mu_{12}^2(\phi_1^\dagger \phi_2 + \phi_2^\dagger \phi_1)$ ². However, implications of a broken S_3 symmetry are outside the scope of this paper.

It is interesting to probe the parameter space arising out of such a vev alignment by proposing H_1 and H_2 as possible DM candidates. For the S_3 HDM to qualify as a good DM model, its predictions of relic-density and direct detection rates must be matched against corresponding experimental data. We arrange for the hierarchy $m_{H_1} < m_{A_1}, m_{H_1^+}$ throughout our numerical analysis (H_1 and A_1 are similar to each other in terms of the masses and couplings, the only difference being the sign of λ_7 . Thus a flip in the sign of λ_7 would tantamount to interchanging H_1 and A_1 . In that case, A_1 would be the DM candidate and the hierarchy required would be $m_{A_1} \leq m_{H_1}, m_{H_1^+}$. The overall physics thus remains unchanged.). LEP constraints on the direct search for charged and pseudoscalar Higgs bosons are evaded by taking $m_{H_i^+}$ and $m_{A_i} > 100$ GeV [40]. Similar to the previous case, we describe the model parameter space in terms of the physical parameters $\{\lambda_1, \lambda_2, \lambda_3, m_{H_1}, m_{A_1}, m_{H_1^+}, \lambda_L\}$.

Our main motivation is to study the high-scale stability of the S_3 HDM for the two different vev assignments discussed above. In doing that we juxtapose the constraints coming from oblique parameters, Higgs signal strengths in the first case, and also the ones coming from relic-density and direct detection in the second case. In principle there can be other such vev configurations as well, and our choice is not exhaustive in that sense. Nonetheless, this paper takes into account two representative cases. The first one defines an *active* 3HDM scenario, i.e, when all three ϕ_1, ϕ_2 and ϕ_3 receive non-zero vevs. The second one describes an *inert* scenario, where these inert scalars do not mix with the 125 GeV Higgs that comes from ϕ_3 .

²The degeneracy persists even after one-loop radiative effects are incorporated. This is because the Z_2 symmetry that emerges unbroken after EWSB is an exact symmetry not only of the scalar potential, but of the entire lagrangian. Thus, this not only leads to equal tree level masses, but also equal couplings for H_1 and H_2 . The two-point correlators for H_1 and H_2 , $\Pi_{H_1 H_1}(p)$ and $\Pi_{H_2 H_2}(p)$ (say) respectively, would have exactly the same expressions then. This would lead to equal one-loop corrected masses for H_1 and H_2 . In other words, the unbroken Z_2 symmetry would protect the degeneracy at the one-loop level.

2.2 Yukawa Sector.

The most general Yukawa lagrangian consistent with the gauge and S_3 symmetries, for the up-type quarks is given by,

$$\begin{aligned}
-\mathcal{L}_Y^u &= y_1^u \left(\bar{Q}_1 \tilde{\phi}_3 u_{1R} + \bar{Q}_2 \tilde{\phi}_3 u_{2R} \right) + y_2^u \left\{ \left(\bar{Q}_1 \tilde{\phi}_2 + \bar{Q}_2 \tilde{\phi}_1 \right) u_{1R} + \left(\bar{Q}_1 \tilde{\phi}_1 + \bar{Q}_2 \tilde{\phi}_2 \right) u_{2R} \right\} \\
&\quad + y_3^u \bar{Q}_3 \tilde{\phi}_3 u_{3R} + y_4^u \bar{Q}_3 \left(\tilde{\phi}_1 u_{1R} + \tilde{\phi}_2 u_{2R} \right) + y_5^u \left(\bar{Q}_1 \tilde{\phi}_1 + \bar{Q}_2 \tilde{\phi}_2 \right) u_{3R} + \text{h.c.}
\end{aligned} \tag{2.11}$$

The lower component of the $SU(2)$ doublets of Higgs multiplets are uncharged in the convention we use. A standard abbreviation reads $\tilde{\phi}_i = i\sigma_2 \phi_i^*$. The Yukawa couplings of the d_R quarks can be obtained by replacing u_{iR} by d_{iR} , y_i^u by y_i^d , and $\tilde{\phi}_i$ by ϕ_i in \mathcal{L}_Y^u and similarly for leptons. The Yukawa couplings are in general complex, which can be responsible for CP violation. More elaborate discussions on S_3 symmetric Yukawa textures can be found in [42–45].

After symmetry breaking, the mass matrix that arises in the up-type quark sector is the following, (In the u, c, t basis):

$$\mathcal{M}_u = \begin{pmatrix} (y_1^u v_3 + y_2^u v_2)/\sqrt{2} & y_2^u v_1/\sqrt{2} & y_5^u v_1/\sqrt{2} \\ y_2^u v_1/\sqrt{2} & y_1^u v_3 - y_2^u v_2/\sqrt{2} & y_5^u v_2/\sqrt{2} \\ y_4^u v_1/\sqrt{2} & y_4^u v_2/\sqrt{2} & y_3^u v_3/\sqrt{2} \end{pmatrix}, \quad \text{with } v_1 = \sqrt{3}v_2. \tag{2.12}$$

The texture is of the same form for the down-type quarks and charged leptons. In principle, one can retain all the parameters in the Yukawa matrix and fine-tune them appropriately in order to reproduce the correct fermion masses and mixings. However that would make the analysis using RG complicated and unwieldy and hence, we look for a simplification. Choosing $y_4^u, y_5^u = 0$ brings \mathcal{M}_u to a $2 \times 2 \oplus 1 \times 1$ block-diagonal form. The quark masses in the SM can be straightforwardly reproduced by diagonalising the remaining the 2×2 block and then tuning the parameters appropriately. For example, the choice $y_1^u < y_2^u < y_3^u$ reproduces the observed up-type quark mass hierarchy. The advantage of this choice is that only $y_3^u = \frac{v}{v_3} y_t^{SM}$ gets a value large enough to cast an impact on the RG evolution, where y_t^{SM} is the SM t-quark Yukawa coupling and, all other Yukawa couplings have a negligible bearing. In addition, even if we invoke a non-zero y_4^u and y_5^u , the observed quark-mixings will always render them small. Exactly this approximation is applied to the bottom quark and lepton sectors also. It is easy to see that then $y_3^u : y_3^b : y_3^l = m_t : m_b : m_\tau$, i.e, this particular approximation scheme preserves the hierarchy of Yukawa couplings observed in the SM. Hence we infer that only the t -quark can contribute significantly to the beta functions through the parameter y_3^u and the effect of all other fermions can be safely neglected in this context. Thus effectively with only one Yukawa into the picture, as far as high-scale stability is concerned, it becomes easier to throw light on the scalar sector.

In the inert case, all the fermion generations are S_3 -singlets and hence couple only to ϕ_3 .

3 Constraints imposed.

Parameter space of the scenario at hand is surveyed throughly by generating random model-points in the $\{\tan\beta, m_{H_1^+}, m_{H_2^+}, m_{A_1}, m_{A_2}, m_{H_1}, m_{H_2}, c_{\beta-\alpha}\}$ basis in scenario A and, $\{\lambda_1, \lambda_2, \lambda_3, m_{H_1}, m_{A_1}, m_{H_1^+}, \lambda_L\}$ in scenario B. We discuss below the various theoretical and experimental constraints imposed to shape the results.

3.1 Theoretical constraints.

The S_3 HDM remains a calculable theory if the model parameters fulfil the respective perturbativity constraints, $|\lambda_i| \leq 4\pi$, $|y_t|, |g_1|, |g_2|, |g_3| \leq \sqrt{4\pi}$. A more stringent choice is to demand all of the couplings $\leq \sqrt{4\pi}$. We however stick to 4π , since this projects out the maximally allowed parameter space.

The $2 \rightarrow 2$ amplitude matrix corresponding to scattering of the longitudinal components of the gauge bosons can be mapped to a corresponding matrix for the scattering of the goldstone bosons [46–49]. The theory respects unitarity if each eigenvalue of the aforementioned amplitude matrix does not exceed 8π .

$$|a_i^\pm|, |b_i| \leq 8\pi, \text{ for } i = 1, 2, \dots, 6. \quad (3.1)$$

The expressions for the individual eigenvalues [39] in terms of quartic couplings are given below :

$$a^\pm = \left(\lambda_1 - \lambda_2 + \frac{\lambda_5 + \lambda_6}{2} \right) \pm \sqrt{\left(\lambda_1 - \lambda_2 + \frac{\lambda_5 + \lambda_6}{2} \right)^2 - 4 \left\{ (\lambda_1 - \lambda_2) \left(\frac{\lambda_5 + \lambda_6}{2} \right) - \lambda_4^2 \right\}}, \quad (3.2a)$$

$$b^\pm = (\lambda_1 + \lambda_2 + 2\lambda_3 + \lambda_8) \pm \sqrt{(\lambda_1 + \lambda_2 + 2\lambda_3 + \lambda_8)^2 - 4 \{ \lambda_8(\lambda_1 + \lambda_2 + 2\lambda_3) - 2\lambda_7^2 \}}, \quad (3.2b)$$

$$c^\pm = (\lambda_1 - \lambda_2 + 2\lambda_3 + \lambda_8) \pm \sqrt{(\lambda_1 - \lambda_2 + 2\lambda_3 + \lambda_8)^2 - 4 \left\{ \lambda_8(\lambda_1 - \lambda_2 + 2\lambda_3) - \frac{\lambda_6^2}{2} \right\}}, \quad (3.2c)$$

$$d^\pm = \left(\lambda_1 + \lambda_2 + \frac{\lambda_5}{2} + \lambda_7 \right) \pm \sqrt{\left(\lambda_1 + \lambda_2 + \frac{\lambda_5}{2} + \lambda_7 \right)^2 - 4 \left\{ (\lambda_1 + \lambda_2) \left(\frac{\lambda_5}{2} + \lambda_7 \right) - \lambda_4^2 \right\}}, \quad (3.2d)$$

$$e^\pm = (5\lambda_1 - \lambda_2 + 2\lambda_3 + 3\lambda_8) \pm \sqrt{(5\lambda_1 - \lambda_2 + 2\lambda_3 + 3\lambda_8)^2 - 4 \left\{ 3\lambda_8(5\lambda_1 - \lambda_2 + 2\lambda_3) - \frac{1}{2}(2\lambda_5 + \lambda_6)^2 \right\}}, \quad (3.2e)$$

$$f^\pm = \left(\lambda_1 + \lambda_2 + 4\lambda_3 + \frac{\lambda_5}{2} + \lambda_6 + 3\lambda_7 \right) \pm \sqrt{\left(\lambda_1 + \lambda_2 + 4\lambda_3 + \frac{\lambda_5}{2} + \lambda_6 + 3\lambda_7 \right)^2 - 4 \left\{ (\lambda_1 + \lambda_2 + 4\lambda_3) \left(\frac{\lambda_5}{2} + \lambda_6 + 3\lambda_7 \right) - 9\lambda_4^2 \right\}}, \quad (3.2f)$$

$$h_1 = \lambda_5 + 2\lambda_6 - 6\lambda_7, \quad (3.2g)$$

$$h_2 = \lambda_5 - 2\lambda_7, \quad (3.2h)$$

$$h_3 = 2(\lambda_1 - 5\lambda_2 - 2\lambda_3), \quad (3.2i)$$

$$h_4 = 2(\lambda_1 - \lambda_2 - 2\lambda_3), \quad (3.2j)$$

$$h_5 = 2(\lambda_1 + \lambda_2 - 2\lambda_3), \quad (3.2k)$$

$$h_6 = \lambda_5 - \lambda_6. \quad (3.2l)$$

In addition to the above, the scalar potential must be bounded from below in order to render the electroweak vacuum stable. Demanding absolute *stability* of the vacuum leads to the following conditions [39],

$$\text{vsc1} : \lambda_1 > 0, \quad (3.3)$$

$$\text{vsc2} : \lambda_8 > 0, \quad (3.4)$$

$$\text{vsc3} : \lambda_1 + \lambda_3 > 0, \quad (3.5)$$

$$\text{vsc4} : 2\lambda_1 + (\lambda_3 - \lambda_2) > |\lambda_2 + \lambda_3|, \quad (3.6)$$

$$\text{vsc5} : \lambda_5 + 2\sqrt{\lambda_8(\lambda_1 + \lambda_3)} > 0, \quad (3.7)$$

$$\text{vsc6} : \lambda_5 + \lambda_6 + 2\sqrt{\lambda_8(\lambda_1 + \lambda_3)} > 2|\lambda_7|, \quad (3.8)$$

$$\text{vsc7} : \lambda_1 + \lambda_3 + \lambda_5 + \lambda_6 + 2\lambda_7 + \lambda_8 > 2|\lambda_4|. \quad (3.9)$$

This conditions can be arrived at by demanding the scalar potential remains positive along various directions in the field space in the $\phi_i \rightarrow \infty$ limit. We do not consider *metastable* vacua configurations in this paper [50, 51], which are expected to project a more relaxed parameter space in this context.

3.2 Oblique parameters.

The S_3 HDM induces modification in the S , T and U parameters through the additional scalars participating in the loops of the gauge-boson self energies. One discerns the 3HDM contribution from the SM as,

$$S = S_{SM} + \Delta S \quad (3.10a)$$

$$T = T_{SM} + \Delta T, \quad (3.10b)$$

$$U = U_{SM} + \Delta U \quad (3.10c)$$

Here ΔS , ΔT and ΔU denote the S_3 HDM contributions. These have been derived following the approach outlined in [52]. Relevant expressions can be found in the Appendix A. The central value is the contribution coming from the standard model with the reference values $m_{h,\text{ref}} = 125.0$ GeV and $M_{t,\text{ref}} = 173.1$ GeV where M_t denotes the pole mass of the top quark. We have used 1σ limits of S, T and U following [53].

3.3 Higgs Signal-strengths

The ATLAS and CMS collaborations have measured the production cross section for a ~ 125 GeV Higgs multiplied by its branching ratios to various possible channels. The results so far are increasingly in favor of the SM predictions. An extended Higgs sector, such as the S_3 HDM although can very well contain a scalar with mass around 125 GeV, but yet can potentially modify the signal strength predictions through its modified higgs-gauge boson and higgs-fermion couplings. For example, the hVV and $h\bar{b}b$ couplings get scaled by $\sin(\beta - \alpha)$ and $\frac{\sin\alpha}{\cos\beta}$ w.r.t the SM, in the case with three non-zero vevs. The loop induced decay widths to $\gamma\gamma$ and $Z\gamma$ final states are also modified. However, one can always arrange for $\alpha = \beta - \frac{\pi}{2}$ which reproduces exact SM couplings. This so called *alignment limit* is present in two-higgs doublet models as well [54]. We explore a case where this limit is not strictly enforced, rather $\sin(\beta - \alpha) = 0.98$ is taken. The reader is reminded that the tree level couplings of h to fermions and gauge bosons remain identical to the SM in the presence of additional inert doublets.

In order to check the consistency of a 2HDM with the measured rates in various channels, we theoretically compute the signal strength μ^i for the i -th channel using the relation:

$$\mu^i = \frac{R_{\text{prod}} \times R_{\text{decay}}^i}{R_{\text{width}}} . \quad (3.11)$$

Here R_{prod} , R_{decay}^i and R_{width} denote respectively the ratios of the theoretically calculated production cross section, the decay rate to the i -th channel and the total decay width for a ~ 125 GeV Higgs to their corresponding SM counterparts. For our numerical analysis, we have taken gluon fusion to be the dominant production mode for the SM-like Higgs.³ The predicted signal-strengths to ZZ , WW , $b\bar{b}$ channels are in

³While other channels such as vector boson fusion (VBF) and associated Higgs production with W/Z (VH) have yielded data in the 8 TeV run, the best fit signal strengths are still dominated by the gluon fusion channel.

excellent agreement with the SM once the alignment limit is invoked. $\mu_{\gamma\gamma}$ still needs to be controlled since the charged scalars do not decouple from the theory in spite of an exact alignment (see Appendix C). In an exact-alignment scenario, the total width of h hardly deviates from its SM value and $\mu_{\gamma\gamma}$ settles approximately to $\frac{\Gamma_{S_3\text{HDM}}^{h\rightarrow\gamma\gamma}}{\Gamma_{\text{SM}}^{h\rightarrow\gamma\gamma}}$. Latest measurements from ATLAS and CMS give $\mu_{\gamma\gamma} = 1.17^{+0.27}_{-0.27}$ and $1.12^{+0.24}_{-0.24}$ respectively [55, 56]. We use the cited limits at 2σ .

We make the passing remark that in-house codes have been employed to carry out the computations related to oblique parameters and signal strengths. In particular, the RG equations have been numerically solved by implementing the Runge-Kutta (RK4) algorithm in the same.

3.4 Dark matter relic density and direct detection

In the one active + two inert doublet case, we impose that the relic density must be away by at most 3σ limits from the PLANCK [57] central value. That is,

$$0.1118 \leq \Omega h^2 \leq 0.1199. \quad (3.12)$$

A more relaxed requirement is to impose only the upper limit, in which case it implies that the S_3 inert scalars only partially account for the observed relic density. Relic density calculations in this work are done using the publicly available code `micrOMEGAs` [58].

Experiments like XENON100 [59], LUX [60] have placed upper limits on WIMP-nucleon scattering cross sections. We again use `micrOMEGAs` to compute the cross sections and adhere to the more stringent constraints by LUX. Given that WIMP-nucleon scattering in this model occurs only through a t -channel h exchange, the cross section computation is plagued by the uncertainty in the strange quark form factor. We have resorted to the `micrOMEGAs` default parameters in this regard. We have imposed an upper bound of 10^{-46} cm^2 on the spin-independent WIMP-nucleon cross section throughout our analysis.

3.5 Evolution under Renormalisation Group.

The main motivation of this paper is to study the behaviour of the $S_3\text{HDM}$ parameters under Renormalisation Group (RG). The *strategy* adopted is, we select parameter points consistent with the constraints discussed above. The parameter space obtained in the process is allowed to evolve under RG. The one loop beta functions employed for this analysis are listed in the appendix. They were derived by demanding scale-invariance of the one-loop corrected scalar potential following [61], and, cross checked by a standard Feynman diagrammatic calculation. Constraints stemming from perturbativity, unitarity and vacuum stability are demanded to be fulfilled throughout the course of evolution, up to some cut-off Λ . There is however, no natural choice for Λ , given the fact we assume that $S_3\text{HDM}$ is the only physics up to this scale. We aim to push Λ to as high as the GUT scale, or the Planck scale, and explore the consequences on our scenario. Incorporation of these constraints in the RG evolution tightens up the parameter space at the electroweak scale.

Discussion of the RG constraints is crucial in context of a non-minimal Higgs sector such as the $S_3\text{HDM}$, owing to the fact that the additional scalars could ameliorate the vacuum instability problem in the SM [62]. However, due to the additional bosonic content, quartic couplings tend to rise fast and hit the *Landau pole* even though vacuum stability is preserved. To strike a balance between these extremes, the model parameters have to be judiciously tuned. This is precisely what we aim to do in context of an $S_3\text{HDM}$.

4 Impact of the constraints on the parameter space.

4.1 Scenario A: $v_1 = \sqrt{3}v_2$.

Model points are sampled randomly through a scan of the parameter space within the specified ranges,

$$\begin{aligned}\tan\beta &\in [0.1, 50] \\ m_{H_1}, m_{H_2} &\in [125 \text{ GeV}, 1000 \text{ GeV}] \\ m_{A_1}, m_{A_2} &\in [100 \text{ GeV}, 1000 \text{ GeV}] \\ m_{H_1^+}, m_{H_2^+} &\in [80 \text{ GeV}, 1000 \text{ GeV}]\end{aligned}$$

Demanding perturbativity at the electroweak scale puts upper bounds on the scalar masses and $\tan\beta$. In particular, all the scalar masses lie below ~ 800 GeV and $\tan\beta \in [0.3, 13.6]$. The upper bounds on the masses and $\tan\beta$ settle at 1 TeV and 17.3 respectively upon relaxing the perturbativity constraint. In that case the bounds are put by unitarity alone, an observation in consonance with the findings in [39]. Any value of $\tan\beta$ outside the quoted limit is responsible for making the theory non-perturbative through the large values it gives to the quartic couplings in the process. This can be revealed through an inspection of Eqn.(2.5).

The next part of the analysis involves evolution under RG. The key finding here is that this scenario is not valid beyond 10^7 GeV. This is attributed to the following two reasons (i) Quartic couplings are large at the input scale itself, they hit the perturbative limit around the multi-TeV scale. This can be understood using the following logic, the quartic couplings at the input scale are typically $\sim \frac{m^2}{v^2}$ (see Eqn.(2.5)), where m refers to any physical S_3 HDM mass. Thus for an m below the TeV scale, at least one quartic coupling becomes large enough to make the theory non-perturbative. (ii) $\tan\beta > 3$ in particular destabilises the vacuum by enhancing the t-Yukawa with respect to its SM value. It so happens that for many parameter points, the Yukawa coupling itself evolves to non-perturbative value below the instability scale, however this is a subleading effect. The T parameter constraint negates a large number of scan points, many of which otherwise clear the RG constraints up to the highest permissible cut-off 10^7 GeV. This we show in Fig.(2). ΔS mostly stays within its 1σ limit. We also prepare the following two benchmark models (Table 1) to reinforce our observation on a violated vacuum stability or unitarity.

Benchmark	$\tan\beta$	$m_{A_1}(\text{GeV})$	$m_{A_2}(\text{GeV})$	$m_{H_1^+}(\text{GeV})$	$m_{H_2^+}(\text{GeV})$	$m_{H_1}(\text{GeV})$	$m_{H_2}(\text{GeV})$
BP1	3.54	265.12	392.00	146.00	105.00	233.77	143.05
BP2	1.02	102.22	167.78	119.80	107.00	214.95	132.35

Table 1: Benchmark points chosen to illustrate the behaviour under RGE. Λ denotes the maximum extrapolation scale up to which vacuum stability and perturbativity are ensured.

BP1 leads to a destabilised vacuum through $\lambda_8 < 0$ occurring below the TeV scale. On the other hand, λ_1 in BP2 rises rapidly and quickly becomes non-perturbative just after crossing 10^6 GeV. The running of λ_8 and λ_1 in the two cases is displayed in Fig.(1).

The bounds finally obtained on λ_i , taking into account the oblique parameter and the diphoton constraints, are summarised in the Table 2.

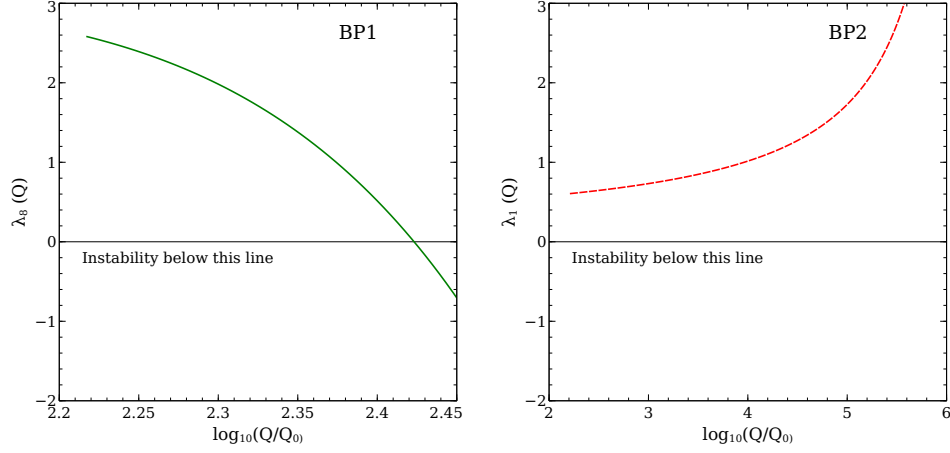


Figure 1: Running of λ_8 corresponding to BP1 (left) and λ_1 corresponding to BP2 (right). $m_h = 125$ GeV and an exact alignment $\sin(\beta - \alpha) = 1.0$ taken in both.

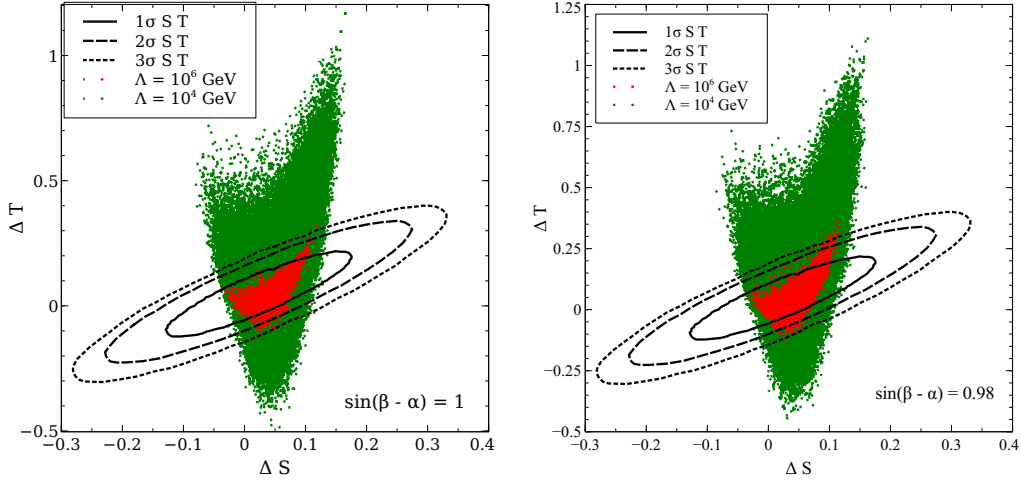


Figure 2: Contribution of the S_3 HDM scalars to the oblique parameters for $\sin(\beta - \alpha) = 1.0$ (Left) and $\sin(\beta - \alpha) = 0.98$ (Right). The ellipses denote the 1σ (solid), 2σ (dashed) and 3σ (dotted) limits. The green and red points indicate validity till 10^4 GeV and 10^6 GeV respectively. We notice that the oblique parameters do not change appreciably for a slight departure from exact alignment.

Parameter	$\Lambda = 10^3$ GeV	$\Lambda = 10^4$ GeV	$\Lambda = 10^6$ GeV
$\lambda_1 \in$	[0, 2.7]	[0, 1.4]	[0, 0.7]
$\lambda_2 \in$	[-2.7, 2.5]	[-1.4, 1.3]	[-0.6, 0.6]
$\lambda_3 \in$	[-2.2, 2.6]	[-1.0, 1.3]	[-0.2, 0.6]
$\lambda_4 \in$	[-2.1, -0.1]	[-0.9, -0.1]	[-0.4, -0.1]
$\lambda_5 \in$	[-2.7, 5.5]	[-1.1, 3.0]	[-0.4, 1.5]
$\lambda_6 \in$	[-5.3, 4.0]	[-2.6, 1.9]	[-1.1, 0.7]
$\lambda_7 \in$	[-2.2, 0.9]	[-1.0, 0.3]	[-0.4, 0]
$\lambda_8 \in$	[0, 3.8]	[0, 1.9]	[0.1, 1.1]

Table 2: Bounds on the quartic couplings, for $\Lambda = 10^3, 10^4, 10^6$ GeV. Oblique parameter and diphoton constraints are also taken into account. We show the numbers up to the first decimal place.

The $h \rightarrow \gamma\gamma$ rate diminishes with respect to the SM throughout the parameter space, however only for a strict imposition of $\sin(\beta - \alpha) = 1$ [39]. We have projected the S_3 HDM $\mu_{\gamma\gamma}$ values versus $m_{H_1^+}$ and $m_{H_2^+}$ in Fig.(3). The dimensionful $hH_i^+H_i^-$ denoted by $g_{hH_i^+H_i^-}$ is conveniently expressed through $g_{hH_i^+H_i^-} = \frac{2\kappa_i m_{H_i^+}^2}{v}$, where κ_i are dimensionless. Whenever $\alpha = \beta - \frac{\pi}{2}$, it is seen that $\kappa_i = -\left(1 + \frac{m_h^2}{2m_{H_i^+}^2}\right)$ [39] (exact expression given in Appendix C). A decrement in $\mu_{\gamma\gamma}$, in an exact alignment case thus becomes inevitable, since both κ_1 and κ_2 are always negative (see Appendix C). In fact, $\mu_{\gamma\gamma}$ never exceeds 0.82 for validity till 10^6 GeV, given that $|\kappa_1|, |\kappa_2| \geq 1.39$ in that case. Following a similar trend, the points valid till $\Lambda = 10^7$ GeV give $\mu_{\gamma\gamma} < 0.63$ and hence are not phenomenologically acceptable. The bounds put on λ_i translate into corresponding bounds on $\tan\beta$ and the non-standard scalar masses, as shown in Fig.4. We point out that while m_{H_2} could be up to 270 GeV for $\Lambda = 10^6$ GeV, the other masses do not exceed 210 GeV for most parameter points. It is to be noted that κ_1 and κ_2 can take either sign for departure from exact alignment, and hence an increment in the diphoton rate is possible there. (See Fig.(3) for $\sin(\beta - \alpha) = 0.98$.)

A generic feature in context of Scenario A is that, the mass parameters m_{11}^2 and m_{33}^2 get traded off through the tadpole conditions, making λ_i expressible in terms of the physical scalars only. Thus for physical scalars luring below 1TeV, λ_i are already $\mathcal{O}(1)$ or even larger at the input scale. This does not lead to a model that is perturbative at a high scale. As a possible remedy, additional mass parameters in the equations relating λ_i to the physical masses could induce cancellations keeping the quartics further small at the EW scale. This could be achieved either through inclusion of quadratic terms violating S_3 , or through invoking an *inert* vev structure where all of m_{11}^2 and m_{33}^2 do get not eliminated. These terms can elevate the non-standard masses to around ~ 1 TeV and can also lead to $\mu_{\gamma\gamma} > 1$. Since a broken S_3 group is beyond the ambit of the present study, we focus on the inert case (Scenario B) in the subsequent section.

4.2 Scenario B: $v_1 = v_2 = 0$, $v_3 = 246$ GeV.

One needs to put $\lambda_4 = 0$ in order to keep the DM stable through an unbroken Z_2 symmetry. Correct relic density is obtained in the mass regimes $m_{H_1} < 80$ GeV and $m_{H_1} > 370$ GeV. We discuss below the

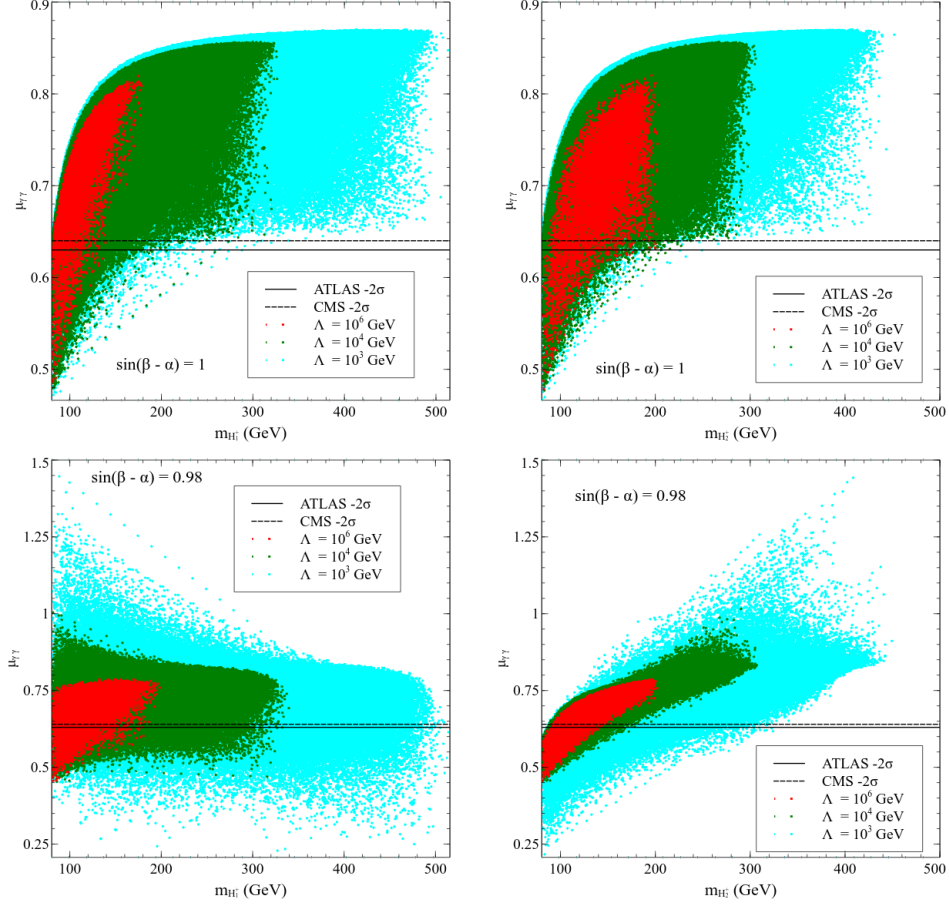


Figure 3: $h \rightarrow \gamma\gamma$ rates for an S_3 HDM valid till a cut-off Λ . The cyan, green and red points are respectively for $\Lambda = 10^3, 10^4$ and 10^6 GeV. The solid and dotted lines denote the 2σ limits below the central value given by ATLAS and CMS respectively .

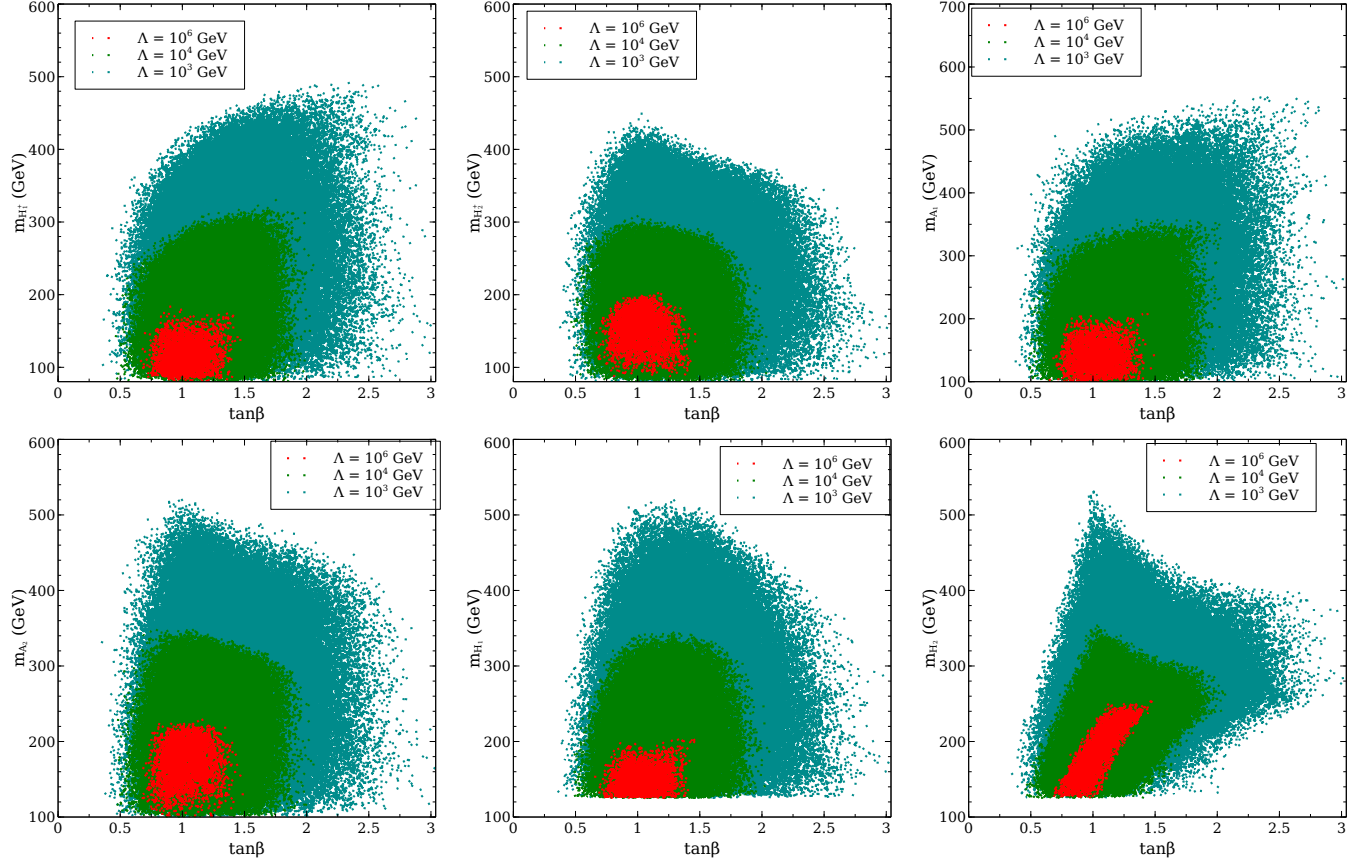


Figure 4: Regions consistent with the theoretical constraints up to a given cut-off. The cyan, green and red points are valid till 10^3 GeV, 10^4 GeV and 10^6 GeV respectively. Oblique parameter and diphoton constraints are also taken into account. Points valid till 10^7 GeV get disallowed by the diphoton constraint and are hence not displayed. An exact alignment is chosen and it has been checked that the bounds do not change for a small deviation from exact alignment.

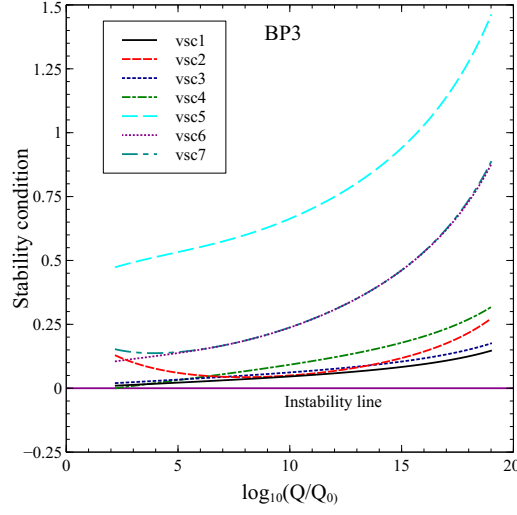


Figure 5: Evolution of BP3 under RG. Colour coding is explained in the legends and the vacuum instability line is highlighted.

phenomenology in detail.

4.2.1 $m_{H_1} < 80$ GeV.

DM particles dominantly annihilate to the $b\bar{b}$ final state through an h in the s-channel, in this mass regime. A sharp decline in relic abundance is noted for $m_{H_1} > 80$ GeV, when the VV (V denoting a vector boson.) mode opens up. Maintaining appropriate mass gaps amongst H_1 , A_1 and H_1^+ turns advantageous in the two following ways. Firstly, the DM relic abundance does not deplete fast through co-annihilations brought in by a narrow mass splitting. Secondly, it gives sizable values to λ_5 , λ_6 and λ_7 which in turn aid to stabilize the vacuum far beyond the SM instability scale, even up to the Planck scale. Overall, the phenomenology in this mass regime is broadly similar to the case with a single inert doublet.

Benchmark	$m_{H_1}(\text{GeV})$	$m_{A_1}(\text{GeV})$	$m_{H_1^+}(\text{GeV})$	λ_L	Ωh^2	$\sigma_{SI}(cm^2)$	$\Lambda(\text{GeV})$
BP3	57.00	102.00	120.00	0.0042	0.1170	4.63×10^{-47}	10^{19}

Table 3: Benchmark point illustrating the behaviour under RGE. Λ denotes the maximum extrapolation scale up to which vacuum stability and perturbativity are ensured.

The displayed benchmark BP3 (Table 3) keeps $\text{BR}(h \rightarrow \text{invisible}) < 19\%$ owing to the tiny λ_L . A perturbative theory at high scales requires m_{A_1} and $m_{H_1^+}$ to obey sharp upper bounds, a feature not reflected by the DM constraints alone. For instance, we need $m_{A_1}, m_{H_1^+} < 135$ GeV in order to salvage perturbativity till the GUT scale.

4.2.2 $m_{H_1} > 370$ GeV.

In this region, dark matter relic density tends to diminish due to prohibitively large annihilation to VV final states. Annihilations in this case are the interference of $H_1 - H_1 - V - V$ four-point coupling and the t/u channel diagrams with H_1^+/A_1 in the propagator. However, a small splitting among the masses of the inert scalars induces cancellation between these two classes of diagrams thereby burgeoning relic density to the desired range. Larger is m_{H_1} , higher is the annihilation to the longitudinal gauge bosons and hence higher becomes λ_L . While a similar phenomenology occurs in case of a single inert doublet, apart from the DM mass < 80 GeV region, Ωh^2 is ~ 0.1 again only when the DM mass > 500 GeV. For example, for $m_{H_1} = 387.5$, $m_{A_1} = 390.5$, $m_{H_1^+} = 389.6$, $\lambda_L = 0.056$, the dominant annihilation channels are $H_1 H_1 \rightarrow WW$ 12%, $H_2 H_2 \rightarrow WW$ 12%, $H_1 H_1 \rightarrow ZZ$ 10%, $H_2 H_2 \rightarrow ZZ$ 10%, $H_1^+ H_1^- \rightarrow WW$ 6%, $H_2^+ H_2^- \rightarrow WW$ 6%, $H_1^+ H_1 \rightarrow \gamma W^+$ 6%, $H_2^+ H_2 \rightarrow \gamma W^+$ 6%. For a spectrum $m_{H_1} = 904.1$, $m_{A_1} = 912.1$, $m_{H_1^+} = 904.3$, the requisite λ_L for a correct relic increases to ~ 0.49 . One thus requires a small mass splitting and an appropriately adjusted λ_L to generate correct relic density.

To examine high-scale validity of this scenario, model points are generated in the following range.

$$\lambda_L \in [-4\pi, 4\pi] \quad (4.1)$$

$$m_{H_1} \in [300.0 \text{ GeV}, 1000.0 \text{ GeV}] \quad (4.2)$$

$$m_{A_1} \in [m_{H_1}, m_{H_1} + 100.0 \text{ GeV}] \quad (4.3)$$

$$m_{H_1^+} \in [m_{H_1}, m_{H_1} + 100.0 \text{ GeV}] \quad (4.4)$$

We also fix $\lambda_1 = \lambda_2 = \lambda_3 = 0.01$ at the initial scale, since these couplings do not enter into the calculations of relic density and WIMP-nucleon cross sections. This choice is rather judicious, an higher value mostly makes the couplings non-perturbative at high scales. Fig.6 displays the variation of relic density corresponding to model points valid up to three different cut-offs $\Lambda = 10^3$ GeV, 10^{16} GeV and 10^{19} GeV. Fig.7 projects spin-independent WIMP-nucleon cross section.

An inspection of Fig.6 and Fig.7 points out that one can render the S_3 HDM stable upto GUT and Planck scales with initial conditions consistent with the observations of relic density and direct detection. We highlight this fact as the most important conclusion in this part. This, however happens only if $m_{H_1} > 550$ GeV. This result be understood as follows. The evolution of λ_8 and hence vacuum stability is crucially dictated by the values of λ_5 , λ_6 and λ_7 at the initial scale. They can be expressed in terms of the masses as,

$$\lambda_5 = \lambda_L + \frac{2}{v^2}(m_{H_1^+}^2 - m_{H_1}^2) \quad (4.5)$$

$$\lambda_6 = \frac{1}{v^2}(m_{H_1}^2 + m_{A_1}^2 - 2m_{H_1^+}^2) \quad (4.6)$$

$$\lambda_7 = \frac{1}{2v^2}(m_{H_1}^2 - m_{A_1}^2) \quad (4.7)$$

We find that for an H_1 below 600 GeV, λ_5 , λ_6 and λ_7 are not sizable enough to ensure $\lambda_8(Q) > 0$ up to the GUT scale. On the other hand, perturbative unitarity restricts the mass splitting to ~ 50 GeV which is automatically consistent with the T parameter constraint. While the stability condition $\lambda_5 + 2\sqrt{\lambda_8(\lambda_1 + \lambda_3)} > 0$ disfavours large negative values of λ_5 , tight upper bounds are imposed by perturbative unitarity. This translates into $-0.1 < \lambda_L < 0.4$ for a model valid up to M_{Pl} (see Fig.6).

For a more comprehensive understanding, the parameter space negotiating all the imposed constraints successfully is displayed as correlation plots in Fig.8. Our demand of $\sigma^{\text{SI}} < 10^{-46} \text{ cm}^2$ throughout in Fig.8

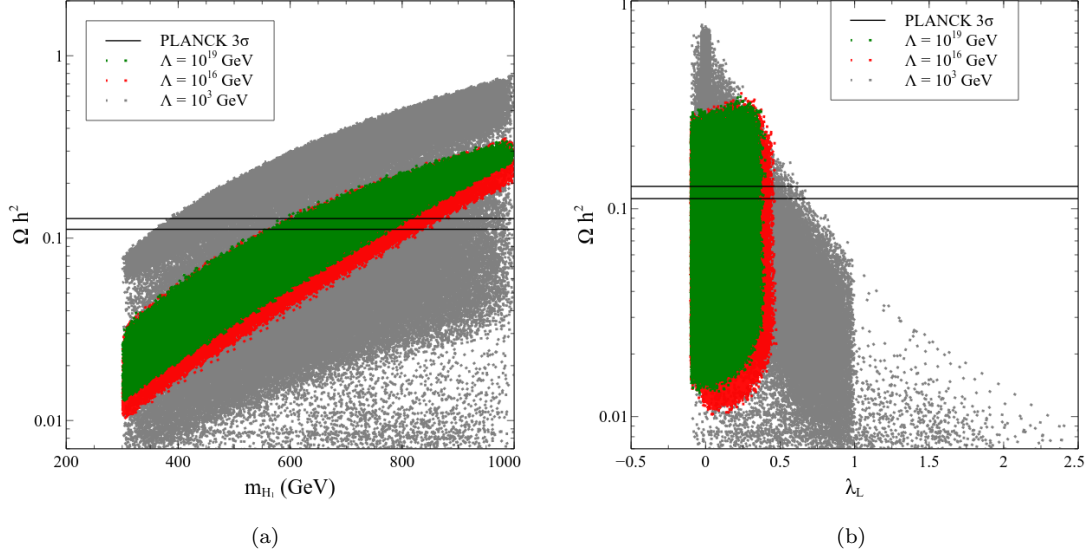


Figure 6: The dark matter relic density versus m_{H_1} (left) and the coupling of H_1 pair to the Higgs boson λ_L (right). The grey, green and red points preserve validity up to 1TeV, the GUT scale 10^{16} GeV and the Planck scale 10^{19} GeV respectively. The horizontal black lines denote the 3σ limits of the PLANCK data. .

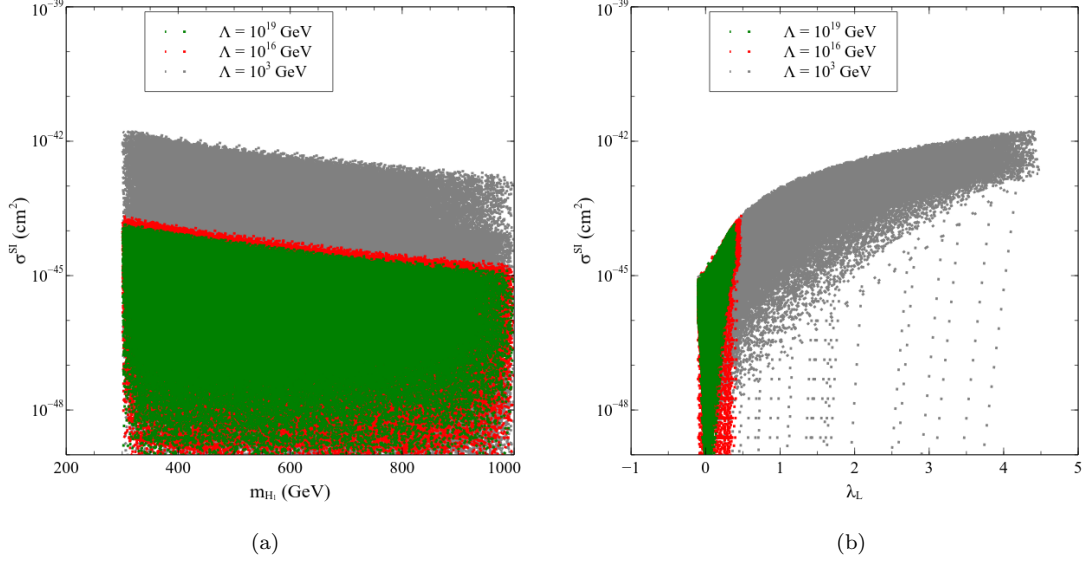


Figure 7: Spin independent WIMP-nucleon scattering cross section vs m_{H_1} (left) and the coupling of H_1 pair to the Higgs boson λ_L (right). The grey, green and red points preserve validity up to 1TeV, the GUT scale 10^{16} GeV and the Planck scale 10^{19} GeV respectively. Note that a large proportion of model points do obey the LUX upper bound while fulfilling stability requirements.

automatically complies with the LUX results. The DM masses are strongly restricted by the requirements of DM searches, and high-scale validity till a given Λ . For instance we note $m_{H_1} \in [550 \text{ GeV}, 830 \text{ GeV}]$ and $[550 \text{ GeV}, 750 \text{ GeV}]$ for $\Lambda = M_{\text{GUT}}$ and $\Lambda = M_{\text{Pl}}$ respectively (see Fig.8).

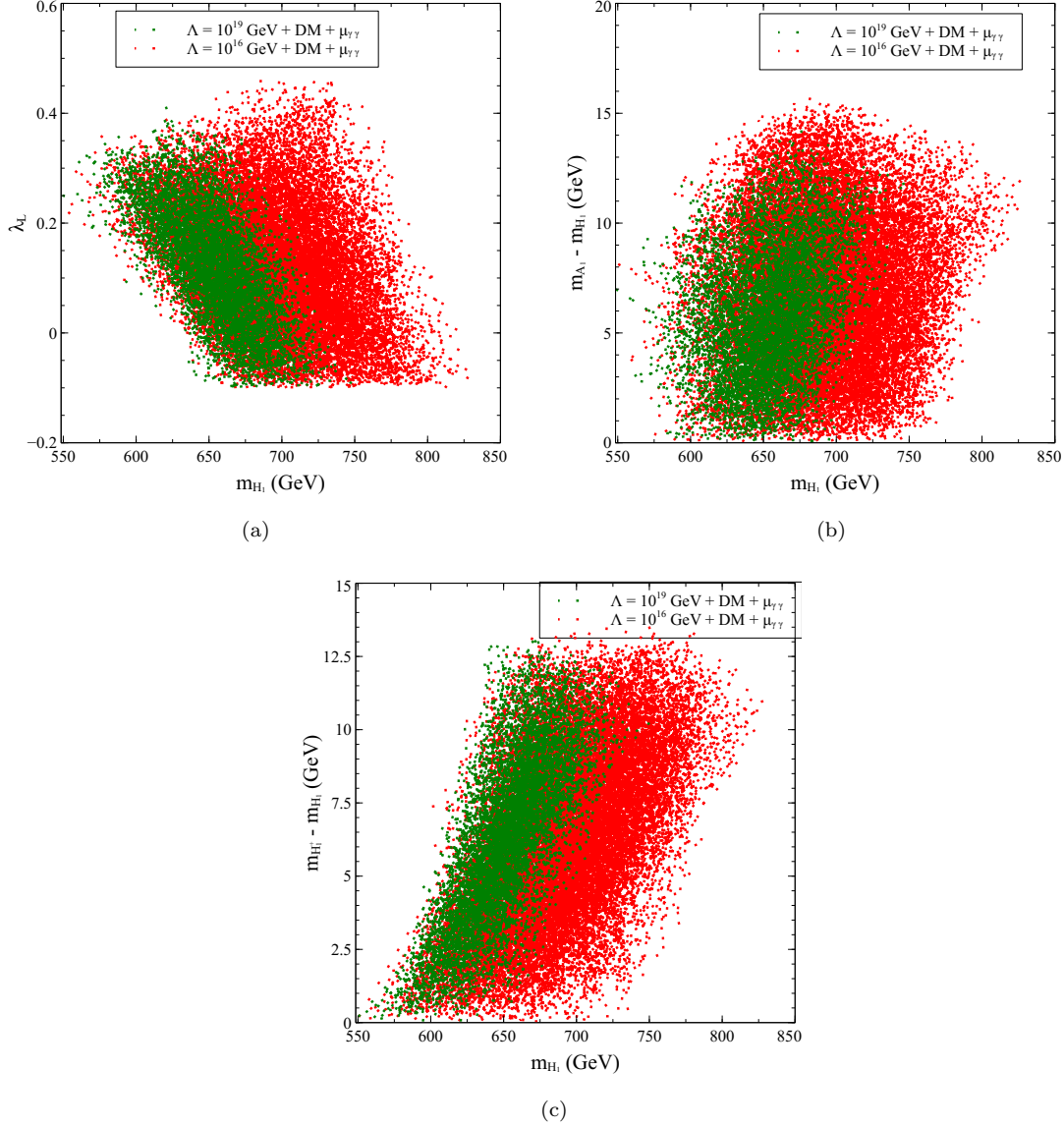


Figure 8: The viable $S_3\text{HDM}$ parameter space projected on the λ_L vs m_{H_1} (top left), $m_{A_1} - m_{H_1}$ vs m_{H_1} (top right), $m_{H_1^+} - m_{H_1}$ vs m_{H_1} (bottom) planes. " $\Lambda + \text{DM} + \mu_{\gamma\gamma}$ " in the legends refers to validity up to Λ as well as consistency with DM searches and diphoton signal strength. The green and red points correspond to $\Lambda = 10^{16} \text{ GeV}$ and $\Lambda = 10^{19} \text{ GeV}$ respectively.

A situation, where $\mu_{\gamma\gamma} < 1$ (Fig.9) for most part of the parameter space is attributed to a mostly non-negative λ_5 (or a very small negative value). The reader should note that unlike the previous case, one can in principle have $\mu_{\gamma\gamma} > 1$ in this case, however subject to stability constraints. With $\lambda_1 = \lambda_3 = 0.01$ at the

input scale, λ_5 gets bounded from below at $\simeq -0.1$ by the vacuum stability condition $\lambda_5 > -2\sqrt{\lambda_8(\lambda_1 + \lambda_3)}$. One can get a deeper lower bound, and hence a $\mu_{\gamma\gamma}$ substantially larger than unity for larger values of λ_1

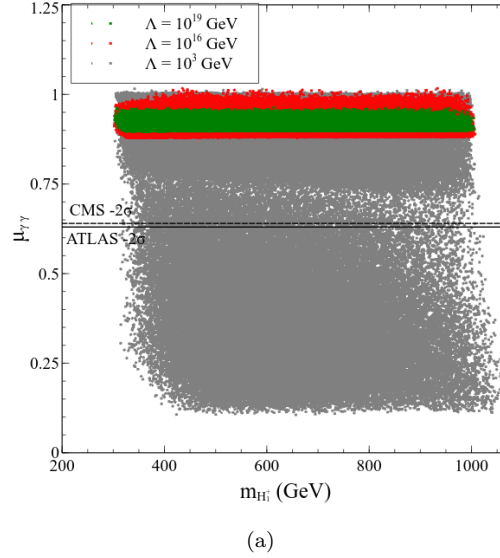


Figure 9: Distribution of parameter points valid till 10^3 GeV (grey), 10^{16} (red) GeV and 10^{19} (green) GeV in the $\mu_{\gamma\gamma}$ vs $m_{H_1^+}$ plane. The solid and dotted lines denote the 2σ limits below the central value given by ATLAS and CMS respectively .

and λ_3 , but in that case one does not have a perturbative theory till 10^{19} GeV. Very low values of $\mu_{\gamma\gamma}$ seen in Fig.9 are possible for points valid only up to the TeV scale, where a positive λ_5 as large as ~ 6.5 is allowed without causing a breakdown of perturbativity below 1TeV. Parameter points valid till the GUT and Planck scales rarely correspond a diphoton signal strength less than 0.87. This indeed is within the 2σ limit from both the ATLAS and CMS central values. This very observation that validity till very high scales always predicts a depletion in the diphoton rate, but still can be kept within the experimental bounds emerges as an important consequence in this regard. The diphoton rate thus bears fingerprints of an extended Higgs sector such as the S_3 HDM, whose tree level couplings could mimic the corresponding SM ones. This calls for its accurate measurements in 13 TeV LHC for instance, or at the other upcoming colliders.

To sum up, DM phenomenology plays a vital role in deciding the fate of this scenario at high scales. The interplay of various effects involved is captured through the benchmarks in Table 4. The RG running of these benchmarks is shown in Fig.10 The first benchmark BP4 can possibly describe physics nearly up to the GUT scale, beyond which perturbativity breaks down. However, BP4 predicts a relic density below the observed limit. This is attributed to the relatively large mass splittings amongst the S_3 scalars, which generate such sizable λ_5 , λ_6 and λ_7 at the initial scale that can ensure $\lambda_8(Q) > 0$ throughout. However we pay the price of a diminished co-annihilation, and thereby a relic density below the desired range. A fall out of this relatively large λ_5 in this case is a suppressed $\mu_{\gamma\gamma}$. BP5 highlights the fact that correct relic density and direct detection rates are achievable in this model for a DM around 390 GeV, a feature not observed in the model with a single inert doublet. The maximal mass difference in such a case is restricted to ~ 13 GeV. However, BP5 does not keep the EW vacuum stable beyond 10^8 GeV.

Benchmark	m_{H_1} (GeV)	m_{A_1} (GeV)	$m_{H_1^+}$ (GeV)	λ_L	Ωh^2	$\sigma_{SI}(cm^2)$	Λ (GeV)
BP4	479.200	480.475	494.525	-0.0236	0.0635	2.13×10^{-47}	10^{19}
BP5	390.000	391.000	392.000	0.0050	0.1200	1.44×10^{-48}	10^8
BP6	707.400	720.000	713.500	0.032	0.1214	1.80×10^{-47}	Just below 10^{16}
BP7	718.600	727.450	727.225	0.0268	0.1263	1.22×10^{-47}	10^{19}

Table 4: Benchmark points chosen to illustrate the behaviour under RGE. Λ denotes the maximum extrapolation scale up to which vacuum stability and perturbativity are ensured.

BP6 and BP7 are conservative choices which predict relic density and direct-detection rates in the correct ballpark, and also extrapolate the model to the GUT and Planck scales respectively. We note here that in BP4, BP6 and BP7, $vsc1$, $vsc3$, $vsc4$, $vsc5$, $vsc6$, $vsc7$ rise with Q , whereas in BP5, $vsc5$ and $vsc6$ go down. This observation has its root in the structure of the S_3 HDM beta functions (see Appendix.A), which mostly guarantee $vsc1$, $vsc3$, $vsc4$, $vsc5$, $vsc6$, $vsc7 > 0$ throughout the evolution once they start with positive values at the EW scale. We remark here that BP6 and BP7 correspond to $\mu_{\gamma\gamma} = 0.935$ and 0.911 respectively, which are within the 2σ limit from the central value.

In the same connection, we have found that an $m_{H_1} > 1$ TeV can render the EW vacuum stable at least up to the SM instability scale. However that pushes μ_{11} to yet higher values, thereby introducing a so-called *intermediate* scale into the picture. It is then implied that the S_3 scalars are practically decoupled below μ_{11} , and that it would be more appropriate to solve the RG equations in a piecewise fashion, i.e., evolve from the EW scale to μ_{11} using the SM beta functions only, and then invoke S_3 HDM above the μ_{11} threshold. However we mostly encounter $\mu_{11} \lesssim 600$ GeV for S_3 masses < 1 TeV. We have checked that for such a μ_{11} , a piecewise evolution practically gives the same numerical results.

5 Conclusions and future work

3HDMs offer a rich scalar spectrum and can give rise to prominent signatures at the colliders [21,22]. In this paper, we have tried to investigate an S_3 -symmetric Higgs sector in the light of various theoretical as well as experimental constraints. Robust regimes of the model parameter space were surveyed using the latest data on the 125 GeV Higgs and oblique parameters. The high-scale behaviour was probed by evolving the model couplings under the RGEs, and this study appears to be the first attempt in that direction in context of 3HDMs. A unitary and perturbative theory, along with a stable EW vacuum was ensured at each step of evolution. We have illustrated our findings in context of two specific alignment of the doublet vevs. The salient features of the numerical results that emerge are highlighted below.

- In the first case, non-zero vevs are assigned to all three of the doublets while maintaining $v_1 = \sqrt{3}v_2$. It is found that this scenario is not stable beyond 10^7 GeV, an effect brought about by an interplay of perturbative unitarity and vacuum stability. Stringent upper bounds are placed on the scalar masses and $\tan\beta$ in this case. In particular we note $\tan\beta < 1.3$ and the S_3 scalar masses lie below 270 GeV for $\Lambda = 10^6$ GeV, the maximum phenomenologically accepted scale.

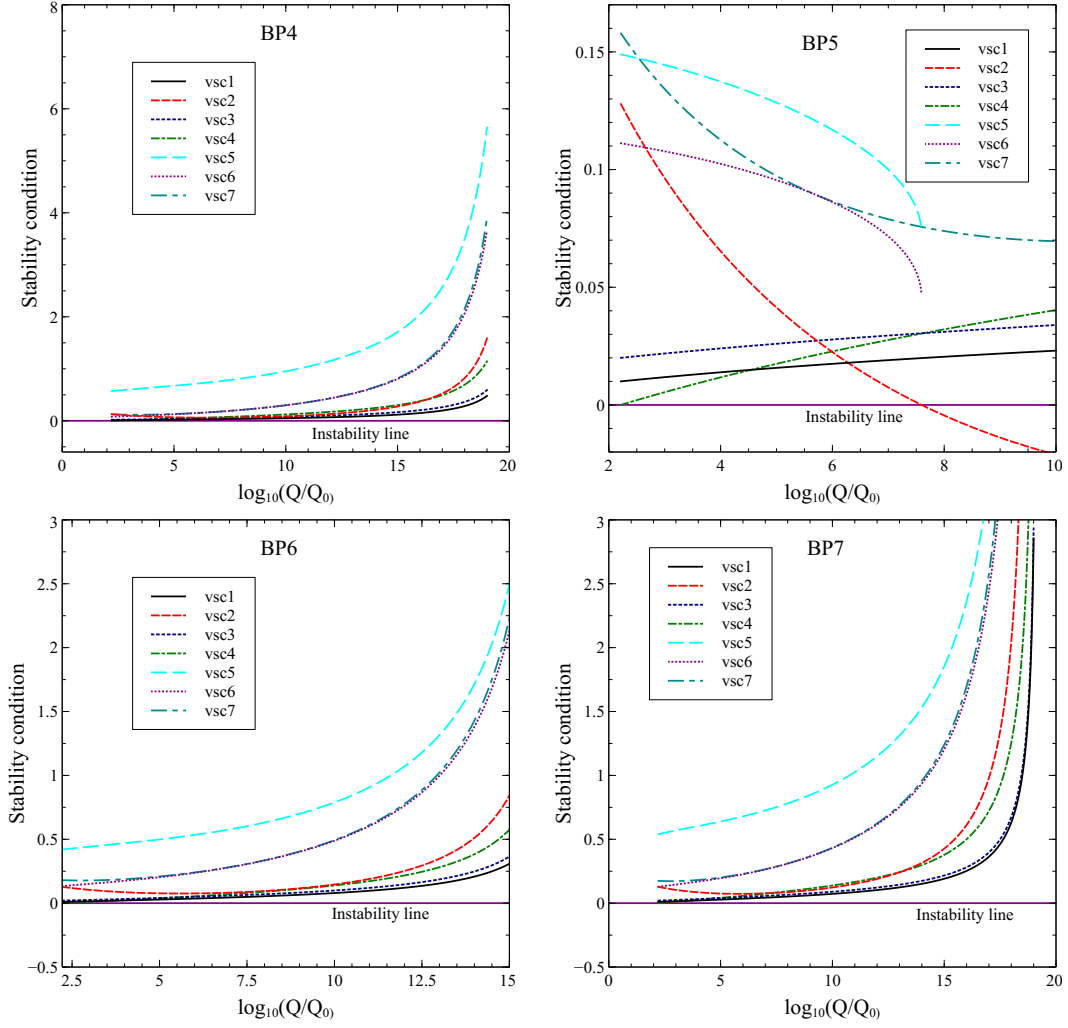


Figure 10: RG Evolution of BP4, BP5, BP6 and BP7. Colour coding is explained in the legends and the vacuum instability line is highlighted. Note that vsc5 and vsc6 are not defined whenever $\lambda_8 < 0$.

- The second case is a scenario with two inert doublets. There lies an identifiable region in the parameter space in this case that extends validity of the model till the Planck scale. Moreover, this parameter space is robust enough to accomodate a successful candidate for dark matter. High-scale stability in this case manifests itself by placing upper bounds on the coupling of the DM to the 125 GeV Higgs, the DM mass, as well on the mass splitting amongst the inert scalars. The bounds get sharper when both the DM as well as high-scale stability constraints are imposed simultaneously. In a word, a connection emerges between DM phenomenology at the *low* scale and a good UV behaviour at *high* scales. This finding is qualitatively similar to the model with a single inert doublet [9]. However, the addition of the extra inert doublet narrows down the gap between the *low* and *high* DM mass regions, with respect to what is observed in the single inert doublet case.
- Scenario B predicts a *decrement* in the diphoton decay width with respect to the SM value, so does Scenario A for an exact alignment. This particular feature of Scenario B is not seen by considering tree-level stability constraints alone and is an explicit consequence of renormalisation group evolution. The numerical predictions however can be made to lie within the current experimental limits without running into conflict with high-scale stability.

Altogether then, we conclude that the inert scenario fares much better than the non-inert one in terms of high-scale validity and signal strength measurements. It is thus safe to comment that the S_3 HDM can certainly alleviate the vacuum stability problem, however not for all permissible vev structures. Several extensions of the present study are possible. One could analyze a more general S_3 -symmetric Yukawa texture in a similar context, admittedly though such texture would give rise to Flavor-Changing Neutral Currents (FCNC) [32] at the tree level. It was shown in [63] that raising the S_3 masses to ~ 10 TeV suppresses the possible FCNCs. The requirement of such heavy scalars necessitates the inclusion of S_3 violating quadratic terms [24]. Another motivation of a broken S_3 symmetry is in the context of DM. In scenario B for instance, it will lead to a non-degenerate spectrum and hence a modified DM phenomenology, at least at the quantitative level. Indirect detection signatures of such a DM scenario could be of special importance in light of latest data. Adding further to it, the large number of bosonic degrees of freedom offered by the S_3 HDM could favour a *strong* first order electroweak phase transition, thereby making way for baryogenesis, something already looked at for a more generic 3HDM with two inert doublets. [64].

6 Acknowledgements

I thank Aritra Gupta for useful discussions, Arijit Dutta for a computational aid, and Biswarup Mukhopadhyaya for his insightful comments on the manuscript. I also acknowledge the funding available from the Department of Atomic Energy, Government of India, for the Regional Centre for Accelerator based Particle Physics (RECAPP), Harish-Chandra Research Institute.

Appendix.

A Renormalisation group (RG) equations

We list the one-loop RG equations for the model couplings used throughout the analysis. For the gauge couplings, they are given by [65],

$$16\pi^2 \frac{dg_s}{dt} = -7g_s^3, \quad (\text{A.1a})$$

$$16\pi^2 \frac{dg}{dt} = -\frac{17}{6}g^3, \quad (\text{A.1b})$$

$$16\pi^2 \frac{dg'}{dt} = \frac{43}{6}g'^3. \quad (\text{A.1c})$$

The quartic couplings evolve according to,

$$16\pi^2 \beta_{\lambda_1} = 32\lambda_1^2 + 8\lambda_2^2 + 16\lambda_3^2 + 4\lambda_4^2 + 2\lambda_5^2 + \frac{1}{2}\lambda_6^2 - 8\lambda_1\lambda_2 + 16\lambda_1\lambda_3 + 2\lambda_5\lambda_6 + 2\lambda_7^2 + \frac{3}{8}(g'^4 + 3g'^2) - \lambda_1(9g^2 + 3g'^2) \quad (\text{A.2a})$$

$$16\pi^2 \beta_{\lambda_2} = 24\lambda_1\lambda_2 - 24\lambda_2^2 - 16\lambda_2\lambda_3 - \frac{1}{2}\lambda_6^2 + 2\lambda_7^2 - \frac{3}{4}g'^2g^2 - \lambda_2(9g^2 + 3g'^2) \quad (\text{A.2b})$$

$$16\pi^2 \beta_{\lambda_3} = 16\lambda_3^2 + 8\lambda_4^2 + 24\lambda_1\lambda_3 + 8\lambda_2\lambda_3 + 8\lambda_4^2 + \frac{1}{2}\lambda_6^2 + 2\lambda_7^2 + \frac{3}{4}g'^2g^2 - \lambda_3(9g^2 + 3g'^2) \quad (\text{A.2c})$$

$$16\pi^2 \beta_{\lambda_4} = \lambda_4(12\lambda_1 + 4\lambda_2 + 24\lambda_3 + 6\lambda_5 + 8\lambda_6 + 20\lambda_7) - \lambda_4(9g^2 + 3g'^2 - 3y_t^2), \quad (\text{A.2d})$$

$$16\pi^2 \beta_{\lambda_5} = 4\lambda_5^2 + 2\lambda_6^2 + 8\lambda_4^2 + 8\lambda_7^2 + 20\lambda_1\lambda_5 - 4\lambda_2\lambda_5 + 8\lambda_3\lambda_5 + 8\lambda_1\lambda_6 + 12\lambda_5\lambda_8 + 4\lambda_6\lambda_8 + \frac{3}{4}(g'^4 - 2g'^2g^2 + 3g^4) - \lambda_5(9g^2 + 3g'^2 - 6y_t^2), \quad (\text{A.2e})$$

$$16\pi^2 \beta_{\lambda_6} = 20\lambda_4^2 + 4\lambda_6^2 + 32\lambda_7^2 + 4\lambda_1\lambda_6 - 4\lambda_2\lambda_6 + 8\lambda_3\lambda_6 + 8\lambda_5\lambda_6 + 4\lambda_8\lambda_6 + 3g'^2g^2 - \lambda_6(9g^2 + 3g'^2 - 6y_t^2), \quad (\text{A.2f})$$

$$16\pi^2 \beta_{\lambda_7} = 4\lambda_7(\lambda_1 + \lambda_2 + 2\lambda_3 + 2\lambda_5 + 3\lambda_6 + \lambda_8) + 10\lambda_4^2 - \lambda_7(9g^2 + 3g'^2 - 6y_t^2), \quad (\text{A.2g})$$

$$16\pi^2 \beta_{\lambda_8} = 4\lambda_5^2 + 4\lambda_5\lambda_6 + 2\lambda_6^2 + 8\lambda_7^2 + 24\lambda_8^2 + \frac{3}{8}(g'^4 + 2g'^2g^2 + 3g^4) - \lambda_8(9g^2 + 3g'^2 - 12y_t^2) - 6y_t^4, \quad (\text{A.2h})$$

Neglecting the effect of other quarks, the t-quark Yukawa coupling has the beta function,

$$16\pi^2 \beta_{y_t} = y_t \left(-8g_s^2 - \frac{9}{4}g^2 - \frac{17}{12}g'^2 + \frac{9}{2}y_t^2 \right) \quad (\text{A.3})$$

B Oblique parameters

The expressions for the oblique parameters in the S_3 HDM are given. A shorthand notation $\sin(\beta - \alpha) = s_{\beta-\alpha}$, $\cos(\beta - \alpha) = c_{\beta-\alpha}$ is adopted,

$$\Delta S = (2s_W^2 - 1)^2 G(m_{H_1^+}^2, m_{H_1^+}^2, m_Z^2) + (2s_W^2 - 1)^2 G(m_{H_2^+}^2, m_{H_2^+}^2, m_Z^2) + G(m_{H_2}^2, m_{A_1}^2, m_Z^2)$$

$$\begin{aligned}
& +c_{\beta-\alpha}^2 G(m_h^2, m_{A_2}^2, m_Z^2) + s_{\beta-\alpha}^2 G(m_{H_1}^2, m_{A_2}^2, m_Z^2) + c_{\beta-\alpha}^2 G(m_{H_1}^2, m_{H_1}^2, m_Z^2) \\
& -s_{\beta-\alpha}^2 G(m_h^2, m_h^2, m_Z^2) - 2\ln(m_{H_1^+}^2) - 2\ln(m_{H_2^+}^2) + \ln(m_{H_2}^2) + \ln(m_{H_1}^2) + \ln(m_{A_1}^2) \\
& +\ln(m_{A_2}^2)
\end{aligned} \tag{B.1a}$$

$$\begin{aligned}
\Delta T = & F(m_{H_1^+}^2, m_{H_2}^2) + F(m_{H_1^+}^2, m_{A_1}^2) + c_{\beta-\alpha}^2 F(m_{H_2^+}^2, m_h^2) + s_{\beta-\alpha}^2 F(m_{H_2^+}^2, m_{H_1}^2) - F(m_{H_2}^2, m_{A_1}^2) \\
& -c_{\beta-\alpha}^2 F(m_h^2, m_{A_2}^2) - s_{\beta-\alpha}^2 F(m_{H_1}^2, m_{A_2}^2) + 3c_{\beta-\alpha}^2 (F(m_Z^2, m_{H_1}^2) - F(m_W^2, m_{H_1}^2)) \\
& -3c_{\beta-\alpha}^2 (F(m_Z^2, m_h^2) - F(m_W^2, m_h^2))
\end{aligned} \tag{B.1b}$$

$$\begin{aligned}
\Delta U = & \frac{1}{24\pi} [G(m_{H_1^+}^2, m_{H_2}^2, m_W^2) + G(m_{H_1^+}^2, m_{A_1}^2, m_W^2) + c_{\beta-\alpha}^2 G(m_{H_2^+}^2, m_h^2, m_W^2) \\
& +s_{\beta-\alpha}^2 G(m_{H_2^+}^2, m_{H_1}^2, m_W^2) + G(m_{H_2^+}^2, m_{A_2}^2, m_W^2) + c_{\beta-\alpha}^2 \hat{G}(m_{H_1}^2, m_W^2) - \hat{G}(m_{H_1}^2, m_Z^2) \\
& -c_{\beta-\alpha}^2 \hat{G}(m_h^2, m_W^2) - \hat{G}(m_h^2, m_Z^2) - G(m_{H_2}^2, m_{A_1}^2, m_Z^2) - c_{\beta-\alpha}^2 G(m_h^2, m_{A_2}^2, m_Z^2) \\
& -s_{\beta-\alpha}^2 G(m_{H_1}^2, m_{A_2}^2, m_Z^2) - (2s_W^2 - 1)^2 G(m_{H_1^+}^2, m_{H_1^+}^2, m_Z^2) \\
& - (2s_W^2 - 1)^2 G(m_{H_2^+}^2, m_{H_2^+}^2, m_Z^2)]
\end{aligned} \tag{B.1c}$$

where,

$$F(m_1^2, m_2^2) \equiv \begin{cases} \frac{m_1^2 + m_2^2}{2} - \frac{m_1^2 m_2^2}{m_1^2 - m_2^2} \ln \frac{m_1^2}{m_2^2} & ; \quad m_1^2 \neq m_2^2, \\ 0 & ; \quad m_1^2 = m_2^2. \end{cases} \tag{B.2}$$

$$\begin{aligned}
G(m_1^2, m_2^2, q^2) \equiv & -\frac{16}{3} + \frac{5(m_1^2 + m_2^2)}{q^2} - \frac{2(m_1^2 - m_2^2)^2}{(q^2)^2} \\
& + \frac{3}{q^2} \left[\frac{m_1^4 + m_2^4}{m_1^2 - m_2^2} - \frac{m_1^4 - m_2^4}{q^2} + \frac{(m_1^2 - m_2^2)^3}{3q^4} \right] \ln \frac{m_1^2}{m_2^2} + \frac{r}{(q^2)^3} f(t, r)
\end{aligned} \tag{B.3}$$

$$\tilde{G}(m_1^2, m_2^2, q^2) \equiv -2 + \left(\frac{m_1^2 - m_2^2}{q^2} - \frac{m_1^2 + m_2^2}{m_1^2 - m_2^2} \right) \ln \frac{m_1^2}{m_2^2} + \frac{f(t, r)}{q^2}. \tag{B.4}$$

$$\hat{G}(m^2, q^2) \equiv G(m^2, m^2, q^2) + 12 \tilde{G}(m^2, m^2, q^2) \tag{B.5}$$

$$t \equiv m_1^2 + m_2^2 - q^2 \quad \text{and} \quad r \equiv (q^2)^2 - 2q^2(m_1^2 + m_2^2) + (m_1^2 - m_2^2)^2 \tag{B.6}$$

$$f(t, r) \equiv \begin{cases} \sqrt{r} \ln \left| \frac{t - \sqrt{r}}{t + \sqrt{r}} \right| & ; \quad r > 0, \\ 0 & ; \quad r = 0, \\ 2\sqrt{-r} \tan^{-1} \frac{\sqrt{-r}}{t} & ; \quad r < 0. \end{cases} \tag{B.7}$$

These are standard functions arising in a one-loop calculation.

C $h \rightarrow \gamma\gamma$ decay width

The partial decay width of the SM-like Higgs to a pair of photons in this case has the expression [66],

$$\Gamma(h \rightarrow \gamma\gamma) = \frac{\alpha^2 g^2}{2^{10} \pi^3} \frac{m_h^3}{M_W^2} \left| \sin(\beta - \alpha) F_W + \left(-\frac{\sin\alpha}{\cos\beta} \right) \frac{4}{3} F_t + \sum_{i=1}^2 \kappa_i F_{i+} \right|^2, \tag{C.1}$$

The functions F_W , F_t and F_{i+} capture the effects of a W-boson, a t-quark and a charged scalar running in the loop and shall be defined as,

$$F_W = 2 + 3\tau_W + 3\tau_W(2 - \tau_W)f(\tau_W), \quad (\text{C.2a})$$

$$F_t = -2\tau_t[1 + (1 - \tau_t)f(\tau_t)], \quad (\text{C.2b})$$

$$F_{i+} = -\tau_{i+}[1 - \tau_{i+}f(\tau_{i+})]. \quad (\text{C.2c})$$

$$f(\tau) = \left[\sin^{-1} \left(\sqrt{1/\tau} \right) \right]^2. \quad (\text{C.3})$$

$$\text{with, } \tau = \frac{4m_a^2}{m_h^2} \quad (\text{C.4})$$

Here, $a = t, W$ and H_i^+ .

For Scenario A:

$$\begin{aligned} \kappa_1 = & -\frac{1}{6v}(2 \cos \alpha \operatorname{cosec} \beta (-6m_{H_1}^2 + 3m_{H_2}^2 - 3m_h^2 + m_{H_2}^2 + 3m_{H_2^+}^2 \cos 2\beta) + \\ & (6m_{H_2^+}^2 + 2m_{H_2}^2 + m_{H_2^+}^2 \cos 2\beta) \sec \beta \sin \alpha), \end{aligned} \quad (\text{C.5a})$$

$$\begin{aligned} \kappa_2 = & \frac{1}{9v}((9(-2m_{H_2^+}^2 + m_h^2) \cos \beta - 9m_h^2 \sec \beta + m_{H_2}^2 \sec^3 \beta) \sin \alpha + \\ & ((9m_h^2 + m_{H_2}^2) \operatorname{cosec} \beta + 18m_{H_2^+}^2 \sin \beta - 9m_h^2 \sin \beta + m_{H_2}^2 \sec \beta \tan \beta) \cos \alpha) \end{aligned} \quad (\text{C.5b})$$

For Scenario B:

$$\kappa_1 = \kappa_2 = -\frac{\lambda_5}{2}. \quad (\text{C.6a})$$

References

- [1] **ATLAS** Collaboration, G. Aad et al., *Observation of a new particle in the search for the Standard Model Higgs boson with the ATLAS detector at the LHC*, *Phys.Lett.* **B716** (2012) 1–29, [[arXiv:1207.7214](#)].
- [2] **CMS** Collaboration, S. Chatrchyan et al., *Observation of a new boson at a mass of 125 GeV with the CMS experiment at the LHC*, *Phys.Lett.* **B716** (2012) 30–61, [[arXiv:1207.7235](#)].
- [3] A. Freitas and P. Schwaller, *Higgs CP Properties From Early LHC Data*, *Phys. Rev.* **D87** (2013), no. 5 055014, [[arXiv:1211.1980](#)].
- [4] A. Djouadi, R. M. Godbole, B. Mellado, and K. Mohan, *Probing the spin-parity of the Higgs boson via jet kinematics in vector boson fusion*, *Phys. Lett.* **B723** (2013) 307–313, [[arXiv:1301.4965](#)].
- [5] A. Djouadi and G. Moreau, *The couplings of the Higgs boson and its CP properties from fits of the signal strengths and their ratios at the 7+8 TeV LHC*, *Eur. Phys. J.* **C73** (2013), no. 9 2512, [[arXiv:1303.6591](#)].
- [6] G. Degrandi, S. Di Vita, J. Elias-Miro, J. R. Espinosa, G. F. Giudice, G. Isidori, and A. Strumia, *Higgs mass and vacuum stability in the Standard Model at NNLO*, *JHEP* **08** (2012) 098, [[arXiv:1205.6497](#)].

- [7] D. Buttazzo, G. Degrandi, P. P. Giardino, G. F. Giudice, F. Sala, A. Salvio, and A. Strumia, *Investigating the near-criticality of the Higgs boson*, *JHEP* **12** (2013) 089, [[arXiv:1307.3536](#)].
- [8] G. Bertone, D. Hooper, and J. Silk, *Particle dark matter: Evidence, candidates and constraints*, *Phys. Rept.* **405** (2005) 279–390, [[hep-ph/0404175](#)].
- [9] A. Goudelis, B. Herrmann, and O. Stl, *Dark matter in the Inert Doublet Model after the discovery of a Higgs-like boson at the LHC*, *JHEP* **09** (2013) 106, [[arXiv:1303.3010](#)].
- [10] A. Aranda, C. Bonilla, and J. L. Diaz-Cruz, *Three generations of Higgses and the cyclic groups*, *Phys. Lett.* **B717** (2012) 248–251, [[arXiv:1204.5558](#)].
- [11] I. de Medeiros Varzielas, O. Fischer, and V. Maurer, *A_4 symmetry at colliders and in the universe*, *JHEP* **08** (2015) 080, [[arXiv:1504.03955](#)].
- [12] S. Moretti, D. Rojas, and K. Yagyu, *Enhancement of the $H^\pm W^\mp Z$ vertex in the three scalar doublet model*, *JHEP* **08** (2015) 116, [[arXiv:1504.06432](#)].
- [13] I. P. Ivanov and E. Vdovin, *Discrete symmetries in the three-Higgs-doublet model*, *Phys. Rev.* **D86** (2012) 095030, [[arXiv:1206.7108](#)].
- [14] M. Maniatis, D. Mehta, and C. M. Reyes, *Stability and symmetry breaking in a three-Higgs-doublet model with lepton family symmetry $O(2)\mathbb{Z}_2$* , *Phys. Rev.* **D92** (2015), no. 3 035017, [[arXiv:1503.05948](#)].
- [15] S. Moretti and K. Yagyu, *Constraints on Parameter Space from Perturbative Unitarity in Models with Three Scalar Doublets*, *Phys. Rev.* **D91** (2015) 055022, [[arXiv:1501.06544](#)].
- [16] I. P. Ivanov and E. Vdovin, *Classification of finite reparametrization symmetry groups in the three-Higgs-doublet model*, *Eur. Phys. J.* **C73** (2013), no. 2 2309, [[arXiv:1210.6553](#)].
- [17] S. Pramanick and A. Raychaudhuri, *An A_4 -based see-saw model for realistic neutrino mass and mixing*, [arXiv:1508.02330](#).
- [18] V. Keus, S. F. King, S. Moretti, and D. Sokolowska, *Observable Heavy Higgs Dark Matter*, *JHEP* **11** (2015) 003, [[arXiv:1507.08433](#)].
- [19] V. Keus, S. F. King, S. Moretti, and D. Sokolowska, *Dark Matter with Two Inert Doublets plus One Higgs Doublet*, *JHEP* **11** (2014) 016, [[arXiv:1407.7859](#)].
- [20] V. Keus, S. F. King, and S. Moretti, *Three-Higgs-doublet models: symmetries, potentials and Higgs boson masses*, *JHEP* **01** (2014) 052, [[arXiv:1310.8253](#)].
- [21] G. Bhattacharyya, P. Leser, and H. Pas, *Novel signatures of the Higgs sector from S_3 flavor symmetry*, *Phys. Rev.* **D86** (2012) 036009, [[arXiv:1206.4202](#)].
- [22] G. Bhattacharyya, P. Leser, and H. Pas, *Exotic Higgs boson decay modes as a harbinger of S_3 flavor symmetry*, *Phys. Rev.* **D83** (2011) 011701, [[arXiv:1006.5597](#)].

- [23] E. Barradas-Guevara, O. Flix-Beltrn, and E. Rodriguez-Juregui, *Trilinear self-couplings in an $S(3)$ flavored Higgs model*, *Phys. Rev.* **D90** (2014), no. 9 095001, [[arXiv:1402.2244](#)].
- [24] J. Kubo, H. Okada, and F. Sakamaki, *Higgs potential in minimal $S(3)$ invariant extension of the standard model*, *Phys. Rev.* **D70** (2004) 036007, [[hep-ph/0402089](#)].
- [25] Y. Koide, *Permutation symmetry $S(3)$ and VEV structure of flavor-triplet Higgs scalars*, *Phys. Rev.* **D73** (2006) 057901, [[hep-ph/0509214](#)].
- [26] A. C. B. Machado and V. Pleitez, *Natural Flavour Conservation in a three Higg-doublet Model*, [arXiv:1205.0995](#).
- [27] P. F. Harrison and W. G. Scott, *Permutation symmetry, tri - bimaximal neutrino mixing and the $S3$ group characters*, *Phys. Lett.* **B557** (2003) 76, [[hep-ph/0302025](#)].
- [28] J. Kubo, A. Mondragon, M. Mondragon, and E. Rodriguez-Jauregui, *The Flavor symmetry*, *Prog. Theor. Phys.* **109** (2003) 795–807, [[hep-ph/0302196](#)]. [Erratum: *Prog. Theor. Phys.* 114, 287 (2005)].
- [29] T. Teshima, *Flavor mass and mixing and $S(3)$ symmetry: An $S(3)$ invariant model reasonable to all*, *Phys. Rev.* **D73** (2006) 045019, [[hep-ph/0509094](#)].
- [30] Y. Koide, *$S(3)$ symmetry and neutrino masses and mixings*, *Eur. Phys. J.* **C50** (2007) 809–816, [[hep-ph/0612058](#)].
- [31] S.-L. Chen, M. Frigerio, and E. Ma, *Large neutrino mixing and normal mass hierarchy: A Discrete understanding*, *Phys. Rev.* **D70** (2004) 073008, [[hep-ph/0404084](#)]. [Erratum: *Phys. Rev.* D70, 079905 (2004)].
- [32] A. Mondragon, M. Mondragon, and E. Peinado, *Lepton masses, mixings and FCNC in a minimal $S(3)$ -invariant extension of the Standard Model*, *Phys. Rev.* **D76** (2007) 076003, [[arXiv:0706.0354](#)].
- [33] E. C. F. S. Fortes, A. C. B. Machado, J. Montao, and V. Pleitez, *Scalar dark matter candidates in a two inert Higgs doublet model*, *J. Phys.* **G42** (2015), no. 10 105003, [[arXiv:1407.4749](#)].
- [34] A. Aranda, C. Bonilla, F. de Anda, A. Delgado, and J. Hernandez-Sanchez, *Higgs decay into two photons from a 3HDM with flavor symmetry*, *Phys. Lett.* **B725** (2013) 97–100, [[arXiv:1302.1060](#)].
- [35] I. P. Ivanov and C. C. Nishi, *Symmetry breaking patterns in 3HDM*, *JHEP* **01** (2015) 021, [[arXiv:1410.6139](#)].
- [36] A. P. Serebrov et al., *New measurements of the neutron electric dipole moment*, *JETP Lett.* **99** (2014) 4–8, [[arXiv:1310.5588](#)].
- [37] N. Chakrabarty, U. K. Dey, and B. Mukhopadhyaya, *High-scale validity of a two-Higgs doublet scenario: a study including LHC data*, *JHEP* **12** (2014) 166, [[arXiv:1407.2145](#)].
- [38] O. F. Beltrn, M. Mondragn, and E. Rodriguez-Juregui, *Conditions for vacuum stability in an $s 3$ extension of the standard model*, *Journal of Physics: Conference Series* **171** (2009), no. 1 012028.

- [39] D. Das and U. K. Dey, *Analysis of an extended scalar sector with S_3 symmetry*, *Phys. Rev.* **D89** (2014), no. 9 095025, [[arXiv:1404.2491](#)]. [Erratum: *Phys. Rev.* D91,no.3,039905(2015)].
- [40] **OPAL, DELPHI, L3, ALEPH, LEP Higgs Working Group for Higgs boson searches** Collaboration, *Search for charged Higgs bosons: Preliminary combined results using LEP data collected at energies up to 209-GeV*, in *Lepton and photon interactions at high energies. Proceedings, 20th International Symposium, LP 2001, Rome, Italy, July 23-28, 2001*, 2001. [hep-ex/0107031](#).
- [41] A. Arhrib, Y.-L. S. Tsai, Q. Yuan, and T.-C. Yuan, *An Updated Analysis of Inert Higgs Doublet Model in light of the Recent Results from LUX, PLANCK, AMS-02 and LHC*, *JCAP* **1406** (2014) 030, [[arXiv:1310.0358](#)].
- [42] D. Das, U. K. Dey, and P. B. Pal, *S_3 symmetry and the CKM matrix*, [arXiv:1507.06509](#).
- [43] F. Gonzalez Canales, A. Mondragn, M. Mondragn, U. J. Saldaa Salazar, and L. Velasco-Sevilla, *Quark sector of S_3 models: classification and comparison with experimental data*, *Phys. Rev.* **D88** (2013) 096004, [[arXiv:1304.6644](#)].
- [44] E. Ma and B. Melic, *Updated S_3 model of quarks*, *Phys. Lett.* **B725** (2013) 402–406, [[arXiv:1303.6928](#)].
- [45] T. Teshima and Y. Okumura, *Quark/lepton mass and mixing in S_3 invariant model and CP-violation of neutrino*, *Phys. Rev.* **D84** (2011) 016003, [[arXiv:1103.6127](#)].
- [46] B. W. Lee, C. Quigg, and H. B. Thacker, *Weak interactions at very high energies: The role of the higgs-boson mass*, *Phys. Rev. D* **16** (Sep, 1977) 1519–1531.
- [47] A. G. Akeroyd, A. Arhrib, and E.-M. Naimi, *Note on tree level unitarity in the general two Higgs doublet model*, *Phys. Lett.* **B490** (2000) 119–124, [[hep-ph/0006035](#)].
- [48] J. Horejsi and M. Kladiva, *Tree-unitarity bounds for THDM Higgs masses revisited*, *Eur. Phys. J.* **C46** (2006) 81–91, [[hep-ph/0510154](#)].
- [49] B. Gorczyca and M. Krawczyk, *Tree-Level Unitarity Constraints for the SM-like 2HDM*, [arXiv:1112.5086](#).
- [50] V. Branchina and E. Messina, *Stability, Higgs Boson Mass and New Physics*, *Phys. Rev. Lett.* **111** (2013) 241801, [[arXiv:1307.5193](#)].
- [51] V. Branchina, E. Messina, and M. Sher, *Lifetime of the electroweak vacuum and sensitivity to planck scale physics*, *Phys. Rev. D* **91** (Jan, 2015) 013003.
- [52] W. Grimus, L. Lavoura, O. M. Ogreid, and P. Osland, *The Oblique parameters in multi-Higgs-doublet models*, *Nucl. Phys.* **B801** (2008) 81–96, [[arXiv:0802.4353](#)].
- [53] M. Baak and R. Kogler, *The global electroweak Standard Model fit after the Higgs discovery*, in *Proceedings, 48th Rencontres de Moriond on Electroweak Interactions and Unified Theories*, pp. 349–358, 2013. [arXiv:1306.0571](#). [45(2013)].

- [54] J. F. Gunion and H. E. Haber, *The CP conserving two Higgs doublet model: The Approach to the decoupling limit*, *Phys. Rev.* **D67** (2003) 075019, [[hep-ph/0207010](#)].
- [55] **ATLAS** Collaboration, G. Aad et al., *Measurement of Higgs boson production in the diphoton decay channel in pp collisions at center-of-mass energies of 7 and 8 TeV with the ATLAS detector*, *Phys. Rev.* **D90** (2014), no. 11 112015, [[arXiv:1408.7084](#)].
- [56] **CMS** Collaboration, V. Khachatryan et al., *Precise determination of the mass of the Higgs boson and tests of compatibility of its couplings with the standard model predictions using proton collisions at 7 and 8 TeV*, *Eur. Phys. J.* **C75** (2015), no. 5 212, [[arXiv:1412.8662](#)].
- [57] **Planck** Collaboration, P. A. R. Ade et al., *Planck 2013 results. XVI. Cosmological parameters*, *Astron. Astrophys.* **571** (2014) A16, [[arXiv:1303.5076](#)].
- [58] G. Belanger, F. Boudjema, A. Pukhov, and A. Semenov, *micrOMEGAs₃: A program for calculating dark matter observables*, *Comput. Phys. Commun.* **185** (2014) 960–985, [[arXiv:1305.0237](#)].
- [59] **XENON100** Collaboration, E. Aprile et al., *Dark Matter Results from 225 Live Days of XENON100 Data*, *Phys. Rev. Lett.* **109** (2012) 181301, [[arXiv:1207.5988](#)].
- [60] **LUX** Collaboration, D. S. Akerib et al., *First results from the LUX dark matter experiment at the Sanford Underground Research Facility*, *Phys. Rev. Lett.* **112** (2014) 091303, [[arXiv:1310.8214](#)].
- [61] P. M. Ferreira and D. R. T. Jones, *Bounds on scalar masses in two Higgs doublet models*, *JHEP* **08** (2009) 069, [[arXiv:0903.2856](#)].
- [62] M. Sher, *Electroweak Higgs Potentials and Vacuum Stability*, *Phys. Rept.* **179** (1989) 273–418.
- [63] S. Pakvasa and H. Sugawara, *Discrete symmetry and cabibbo angle*, *Physics Letters B* **73** (1978), no. 1 61 – 64.
- [64] A. Ahriche, G. Faisel, S.-Y. Ho, S. Nasri, and J. Tandean, *Effects of two inert scalar doublets on Higgs boson interactions and the electroweak phase transition*, *Phys. Rev.* **D92** (2015), no. 3 035020, [[arXiv:1501.06605](#)].
- [65] G. C. Branco, P. M. Ferreira, L. Lavoura, M. N. Rebelo, M. Sher, and J. P. Silva, *Theory and phenomenology of two-Higgs-doublet models*, *Phys. Rept.* **516** (2012) 1–102, [[arXiv:1106.0034](#)].
- [66] A. Djouadi, *The Anatomy of electro-weak symmetry breaking. I: The Higgs boson in the standard model*, *Phys. Rept.* **457** (2008) 1–216, [[hep-ph/0503172](#)].